

# SVD-based Causal Emergence for Gaussian Iterative Systems

Kaiwei Liu<sup>1</sup>, Linli Pan<sup>1</sup>, Zhipeng Wang<sup>1</sup>, Bing Yuan<sup>2</sup> and Jiang Zhang<sup>\* 1,2</sup>

<sup>1</sup> School of Systems Science, Beijing Normal University, 100875, Beijing, China

<sup>2</sup>Swarma Research, 102300, Beijing, China

## Abstract

Causal emergence (CE) based on effective information (EI) shows that macro-states can exhibit stronger causal effects than micro-states in dynamics. However, the identification of CE and the maximization of EI both rely on coarse-graining strategies, which is a key challenge. A recently proposed CE framework based on approximate dynamical reversibility utilizing singular value decomposition (SVD) is independent of coarse-graining but is limited to transition probability matrices (TPM) in discrete states. To address this problem, this article proposes a pioneering CE quantification framework for Gaussian iterative systems (GIS), based on approximate dynamical reversibility derived from SVD of covariance matrices in forward and backward dynamics. The positive correlation between SVD-based and EI-based CE, along with the equivalence condition, are given analytically. After that, we can provide precise coarse-graining strategies directly from singular value spectrums and orthogonal matrices. This new framework can be applied to any dynamical system with continuous states and Gaussian noise, such as auto-regressive growth models, Markov Gaussian systems, and even SIR modeling by neural networks (NN). Numerical simulations on typical cases validate our theory and offer a new approach to studying the CE phenomenon, emphasizing noise and covariance over dynamical functions in both known models and machine learning.

*Keywords:* Causal emergence, dynamical reversibility, Gaussian iterative systems, singular value decomposition, covariance matrix.

## 1 Introduction

Complex systems with dynamics are ubiquitous in the world around us, such as ecosystems [1], organisms [2, 3], brains [4–6], cells [7, 8]. The interrelations between different dimensions and the accumulation of randomness result in entropy production and disorder, thereby complicating the analysis of dynamics of microscopic composition such as individuals in society, cells in the human body, and atoms in matter [9, 10]. Many scholars contend that complex systems conceal profound patterns and regularities within their apparent disorder. So they try to derive dynamical models of the systems in macro-level by coarse-graining the dynamical systems, discovering that the strength of the causal effect for macro-states can surpass those of micro-states, a phenomenon called causal emergence (CE) [11–16].

The typical outcome is the quantitative framework for CE based on effective information (EI) proposed by Hoel et al. [12, 13, 17], demonstrating that coarse-grained macro-states may have larger EI than micro-states. The study in Neural Information Squeezer plus (NIS+) [18, 19] based on Hoel’s EI framework, utilizes neural networks (NN) to maximize EI and identify CE in data. After that, an exact theory of CE for Gaussian iterative systems (GIS) [20] expands Hoel’s theory by maximizing EI to derive CE and coarse-graining strategies analytically. However, the dependence on coarse-graining strategies within Hoel’s framework presents challenges. In NIS+, this dependence necessitates training both the dynamics learning module and the encoder for coarse-graining during the machine learning process, significantly reducing computational efficiency. Even the analytical solutions presented in [20] are limited to calculating the solution set of corresponding parameters rather than providing exact values.

Some research is independent of predefined coarse-graining strategies and directly calculates systems’ CE. A notable example is Rosas’ framework [14], which is based on integrated information decomposition theory [21, 22]. In this framework, CE is quantified by calculating the synergic information (*Syn*) across all micro-variables over two consecutive time steps. However, this approach is difficult to implement for the calculation of *Syn* because the combinatorial explosion problem can not be avoided. Although Rosas proposed an approximate method to mitigate the computational complexity, it requires predefined macro-state variables, typically identified through

---

\*Email: zhangjiang@bnu.edu.cn

representation learning [23, 24]. In addition, Barnett and Seth proposed a framework [15] for quantifying CE via dynamical independence, where a system has CE if micro-dynamics do not affect macro-dynamics. Yet, this framework has only been applied to linear systems. Both methods use mutual information, making results sensitive to data distribution and potentially limiting their capture of the system’s essential causal effects.

Zhang et al. recently proposed a CE quantification framework with approximate dynamical reversibility based on singular value decomposition (SVD) [25], which is independent of the optimization of coarse-graining strategies. Approximate dynamical reversibility describes the proximity of probability transition matrices (TPM) to a permutation matrix, CE based on which can be quantified as the potential maximal efficiency increase for approximate dynamical reversibility. This work also finds that the essence of CE lies in redundancy, represented by irreversible and correlated information pathways. It demonstrates a strong correlation between the approximate dynamical reversibility and EI and shows an equivalence between SVD and the EI maximization frameworks for quantifying CE. However, this method only applies to discrete Markov chains with TPM and lacks analytical and exact correlation between SVD-based and EI-based CE. More research is needed to extend this method to general dynamical systems with continuous states, which includes GIS, stochastic differential equations (SDE) [26–28], and NN models.

It is very common to use SVD to study the dynamics of systems. Chen et al. use singular values of the system’s ensemble matrix to find the critical phase transition of the system [29, 30]. In addition to studying the free evolution of systems, Antolus et al. also consider SVD as a key factor in control theory [31–33]. The system can be reduced based on SVD and controlling the dimensions corresponding to the largest few singular values can determine the state transition of the whole system. Similarly, for complex NN models, the memory usage of the parameters can be reduced by retaining only the major singular values of the gradient matrix [34–36]. Traditional SVD focuses on the dynamical function, often overlooking noise and its covariance matrix. However, we find that the covariance matrix also contains crucial information about the system.

Our new research has four motivations. Firstly, CE based on approximate dynamical reversibility under SVD should be extended to GIS, aiming to identify a quantitative approximate equivalence relation between SVD-based and EI-based CE of GIS, along with the conditions under which the equivalences are valid. Secondly, we intend to derive an analytical solution for CE that is independent of coarse-graining for GIS. Next, we hope to find accurate parameters of the coarse-graining strategy instead of a set of optimal solutions for coarse-graining functions. Finally, we want to extend the SVD-based CE theory to NN, which can be used to learn the dynamics in data and compute CE while significantly enhancing operational efficiency.

The main contributions of this article can be divided into four parts. First, we quantify CE based on the approximate dynamical reversibility of GIS [37], extending the reversibility framework via SVD for a discrete Markov chain to GIS. Moreover, this article uses approximate dynamical reversibility based on the SVD of the covariance matrices from forward and backward dynamics, that is, we mainly focused on randomness rather than the parameters of dynamics. Next, we analytically illustrate the approximate correlation between CE frameworks based on SVD and EI and the conditions of their equivalence. Finally, we propose a coarse-graining strategy for GIS utilizing orthogonal matrices in the SVD. Our quantification of CE and coarse-graining strategies applies to various dynamical systems with Gaussian noises, including established GIS models and those data-based models trained by NN, as elaborated in the following section.

## 2 Results

### 2.1 Fundamental theories

#### 2.1.1 Causal emergence based on effective information

We begin with a concise introduction to the Causal Emergence (CE) theory posited by Hoel et al., which is based on the notion of Effective Information (EI) derived from information theory. Concepts about EI were initially introduced by Tononi et al. in [11] and later used by Hoel et al. to quantify CE in [12, 13, 17, 38–41]. For a given transitional probability  $P(x_{t+1}|x_t)$ ,

$$EI = I(x_{t+1}, x_t | do(x_t \sim \mathcal{U}(X))), \quad (2.1)$$

where  $x_t, x_{t+1}, \forall t \geq 0$  represent the state variables defined on  $\mathcal{S}$  at time step  $t$  and  $t + 1$  after the intervention on  $x_t$ , respectively. Where  $do(x_t \sim \mathcal{U}(X))$  is the do operator to intervene in the input variable  $x_t$  to follow a uniform distribution in its domain  $X$  and keep the causal mechanism  $P(x_{t+1}|x_t)$  unchanged.

We have extended the CE framework to stochastic iterative systems under Gaussian noise called GIS in the previous article [20], and many definitions and conclusions were drawn from this. The GIS we discuss is presented as

$$x_{t+1} = a_0 + Ax_t + \varepsilon_t, \varepsilon_t \sim \mathcal{N}(0, \Sigma), \quad (2.2)$$

where,  $a_0, x_t \in \mathcal{R}^n$ ,  $A, \Sigma \in \mathcal{R}^{n \times n}$ . Based on micro-states like Eq.(2.2), we define the macro-state  $y_t = \phi(x_t) = Wx_t$ , where  $W \in \mathcal{R}^{k \times n}$  is the parameter of coarse-graining strategy  $\phi(x_t)$ . The derived macro-state dynamic is,

$$y_{t+1} = a_{M,0} + A_M y_t + \varepsilon_{M,t}, \varepsilon_{M,t} \sim \mathcal{N}(0, \Sigma_M), \quad (2.3)$$

where  $a_{M,0} = Wa_0$ ,  $A_M = WAW^\dagger$ ,  $\Sigma_M = W\Sigma W^T$  and  $k < n$ . In this article,  $(\cdot)^\dagger$  is the Moore-Penrose generalized inverse matrix [42, 43] of  $\cdot$ .

After averaging  $EI$  on the input dimension, we can obtain the dimension averaged effective information  $\mathcal{J}$  for GIS [37, 44] in Definition 2.1, which revised the definition in previous work [20]. Appendix A.1 in Supplementary Information also presents the calculation details.

**Definition 2.1.** (*Dimension averaged effective information for GIS*): For GIS like  $x_{t+1} = a_0 + Ax_t + \varepsilon_t$ ,  $\varepsilon_t \sim \mathcal{N}(0, \Sigma)$ ,  $a_0, x_t \in \mathcal{R}^n$ ,  $A, \Sigma \in \mathcal{R}^{n \times n}$  and  $r \equiv r(A^T \Sigma^{-1} A) \leq r(A) \leq n$ , the **dimension averaged effective information** of the dynamical system is calculated as

$$\mathcal{J} = \frac{EI}{n} = \ln \left( \frac{\text{pdet}(A^T \Sigma^{-1} A)^{\frac{1}{2n}} L}{\sqrt{2\pi e}} \right). \quad (2.4)$$

$\text{pdet}(\cdot)$  represents the generalized determinant value corresponding to matrix  $\cdot$  with rank  $r(\cdot)$  and singular values  $s_i(\cdot)$ ,  $i = 1, \dots, r(\cdot)$ ,  $\text{pdet}(\cdot) = s_1(\cdot)s_2(\cdot)\dots s_{r(\cdot)}(\cdot)$ .  $L$  represents the size of the probability space with a uniform distribution determined by the do-operator  $\text{do}(\cdot)$ , which is an intervention that enforces  $x_t \sim \mathcal{U}([-L/2, L/2]^n)$ , where  $\mathcal{U}$  represents uniform distribution.

According to the properties of information entropy,  $\mathcal{J}$  can be decomposed into two terms as  $\mathcal{J} = \mathcal{J}_1 + \mathcal{J}_2$ , determinism

$$\mathcal{J}_1 = -\ln \left( \sqrt{2\pi e} \det(\Sigma)^{\frac{1}{2n}} \right) \quad (2.5)$$

measures how the current state  $x_t$  can deterministically (sufficiently) influence the state  $x_{t+1}$  in the future, non-degeneracy

$$\mathcal{J}_2 = \ln \left( \text{pdet}(A^T \Sigma^{-1} A)^{\frac{1}{2n}} \det(\Sigma)^{\frac{1}{2n}} L \right), \quad (2.6)$$

measures how exactly we can infer (necessarily) the state  $x_{t-1}$  in the past from the current state  $x_t$ .

Obtaining  $\mathcal{J}$ , we still have a free parameter  $L$ , which is artificially assumed and greatly influences the results of  $\mathcal{J}$ . This hyperparameter can be subtracted by calculating dimensional averaged CE as

$$\Delta\mathcal{J} = \mathcal{J}_M - \mathcal{J}, \quad (2.7)$$

where  $\mathcal{J}_M \equiv \mathcal{J}(A_M, \Sigma_M)$  is the effective information for the macro-dynamics and  $\Delta\mathcal{J}$  is the degree of CE.

After introducing CE  $\Delta\mathcal{J}$  for GIS based on EI, it is obvious that one of its shortcomings is the high dependence on coarse-graining  $\phi(x) = Wx$ ,  $W \in \mathcal{R}^{k \times n}$ ,  $W^\dagger = W^T$ , as

$$\mathcal{J}_M \equiv \mathcal{J}(A_M, \Sigma_M) = \mathcal{J}(WAW^\dagger, W\Sigma W^T). \quad (2.8)$$

Quantifying CE by  $\Delta\mathcal{J}$  requires pre-setting coarse-graining strategies  $\phi$  and optimizing its parameters  $W \in \mathcal{R}^{k \times n}$ ,  $k$  is the pre-defined macro dimension as  $k < n$ , to obtain optimal macro-states and theoretical maximum  $\Delta\mathcal{J}^*$  in [20] as

$$\Delta\mathcal{J}^* = \frac{1}{2k} \sum_{i=1}^k \ln s_i - \frac{1}{2n} \sum_{i=1}^n \ln s_i, \quad (2.9)$$

where  $s_i$ ,  $i = 1, \dots, n$ , are the singular values of  $A^T \Sigma^{-1} A$ . The pre-setting and optimization of  $W$  increases computational complexity and reduces accuracy. Even after the optimization of  $W$ , it is difficult to obtain the optimal  $\Delta\mathcal{J}^*$  in Eq.(2.9) numerically based on data. We need to find a way to explore the potential of CE in GIS directly.

### 2.1.2 SVD-based CE for TPM

Zhang's previous work [25] has provided an indicator of CE for Markov chains called approximate dynamical reversibility, which describes the proximity of a transitional probability matrix (TPM) to a permutation matrix. This new framework for CE is distinctive for its independence from coarse-grained strategies. The calculation of the approximate dynamical reversibility of TPM  $P$  requires solving its singular values as  $P \cdot P^T = VZV^T$  and  $Z = \text{diag}(\zeta_1, \zeta_2, \dots, \zeta_N)$  as  $\zeta_1 \geq \zeta_2 \geq \dots \geq \zeta_N \geq 0$ , then the  $\alpha$ -ordered approximate dynamical reversibility of  $P$  is defined as:

$$\Gamma_\alpha \equiv \sum_i^N \zeta_i^\alpha, \quad (2.10)$$

where  $\alpha \in (0, 2)$  is a parameter. The maximum  $\Gamma_\alpha$  can be achieved if  $P$  is a permutation matrix. Therefore,  $\Gamma_\alpha$  can be used as an index of the reversibility of TPM and an approximate relationship exists as [25]

$$EI \sim \log \Gamma_\alpha. \quad (2.11)$$

Since  $\Gamma_\alpha$  is size-dependent, we need to normalize them by dividing the size of  $P$  as  $\gamma_\alpha = \Gamma_\alpha/N$ , to characterize the size-independent approximate dynamical reversibility. There is an integer  $i \in [1, N]$  such that  $\zeta_i > \epsilon$ , then there is **vague causal emergence** with the level of vagueness  $\epsilon$  occurred in the system as

$$\Delta\Gamma_\alpha(\epsilon) = \frac{\sum_{i=1}^{r_\epsilon} \zeta_i^\alpha}{r_\epsilon} - \frac{\sum_{i=1}^N \zeta_i^\alpha}{N}, \quad (2.12)$$

where  $r_\epsilon = \max\{i | \zeta_i > \epsilon\}$ .  $\epsilon$  can be selected according to the relatively clear cut-offs in the spectrum of singular values. When  $\epsilon = 0$ , if  $r \equiv \text{rank}(P) < N$  then **clear causal emergence** occurs, and the degree is  $\Delta\Gamma_\alpha(0)$ . This definition is independent of any coarse-graining strategy and reflects the inherent property of the Markov chain.

Finally, a concise coarse-graining method based on the SVD of  $P$  to obtain a macro-level reduced TPM can be obtained by projecting the row vectors  $P_i, \forall i \in [1, N]$  in  $P$  onto the sub-spaces spanned by the eigenvectors of  $P \cdot P^T$  such that the major information of  $P$  is conserved, as well as  $\Gamma_\alpha$  is kept unchanged.

## 2.2 Approximate dynamical reversibility of GIS

We can analogy to the approximate dynamical reversibility [25] of TPM to derive the approximate dynamical reversibility of GIS determined by Gaussian mapping [45] like

$$p(x_{t+1}|x_t) = \mathcal{N}(Ax_t + a_0, \Sigma) \equiv \frac{1}{(2\pi)^{\frac{n}{2}} \det(\Sigma)^{\frac{1}{2}}} \exp \left\{ -\frac{1}{2} (x_{t+1} - Ax_t - a_0)^T \Sigma^{-1} (x_{t+1} - Ax_t - a_0) \right\}, \quad (2.13)$$

where,  $A \in \mathcal{R}^{n \times n}$  and  $\Sigma \in \mathcal{R}^{n \times n}$ . In a Markov chain, its TPM is a permutation matrix when the dynamics are reversible. This reversibility can be analogized to GIS. If we treat the Gaussian map defined in Equation (2.30) as a TPM, the state mapping between  $x_t$  and  $x_{t+1}$  is bijective if the TPM is reversible. Here, we need to define the backward dynamics for GIS in Definition 2.2.

**Definition 2.2.** (*Backward dynamics*): For a GIS  $x_{t+1} = a_0 + Ax_t + \varepsilon_t, \varepsilon_t \sim \mathcal{N}(0, \Sigma)$ , also presented as  $p(x_{t+1}|x_t) = \mathcal{N}(Ax_t + a_0, \Sigma)$ , where  $x_t \in \mathcal{R}^n$  to  $x_{t+1} \in \mathcal{R}^n$ ,  $A \in \mathcal{R}^{n \times n}$  and  $\Sigma \in \mathcal{R}^{n \times n}$ , it has a unique backward dynamics

$$x_t = A^\dagger x_{t+1} - A^\dagger a_0 - A^\dagger \varepsilon_t, A^\dagger \varepsilon_t \sim \mathcal{N}(0, A^\dagger \Sigma (A^\dagger)^T). \quad (2.14)$$

$A^\dagger \Sigma (A^\dagger)^T$  is the covariance matrix of backward dynamics as  $A^\dagger$  is the Moore-Penrose generalized inverse matrix of  $A$ .

In continuous space, if the state mapping between two consecutive time points  $x_t$  and  $x_{t+1}$  is bijective,  $r(A) = n$ ,  $\Sigma = 0$  and  $A^\dagger \Sigma (A^\dagger)^T = 0$  needs to be satisfied, then the probability distribution would be a Dirac distribution [46], i.e., all the probability mass is concentrated at a single point as

$$p(x_{t+1}|x_t) = \delta(x_{t+1} - Ax_t - a_0) = \begin{cases} \infty, & x_{t+1} = Ax_t + a_0 \\ 0, & x_{t+1} \neq Ax_t + a_0 \end{cases} \quad (2.15)$$

in which  $\int_{-\infty}^{+\infty} p(x_{t+1}|x_t) dx_{t+1}^n = 1$ ,  $a_0, x_t, x_{t+1} \in \mathcal{R}^n$ ,  $A, \Sigma \in \mathcal{R}^{n \times n}$ . Backward dynamics are the same as  $p(x_t|x_{t+1}) = \delta(x_t - A^\dagger x_{t+1} + A^\dagger a_0)$ . Then, both mappings can be directly written as linear functions  $x_{t+1} = Ax_t + a_0$  and  $x_t = A^\dagger x_{t+1} - A^\dagger a_0$ , where  $A^\dagger = A^{-1}$  in this case.

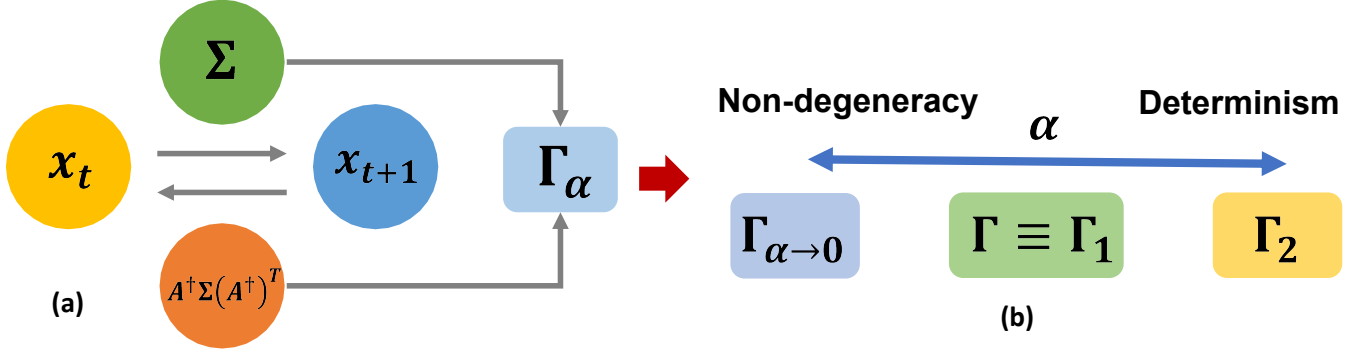


Figure 1: (a) For  $p(x_{t+1}|x_t) = \mathcal{N}(Ax_t + a_0, \Sigma)$ , the covariance matrices of forward dynamics  $x_{t+1} = a_0 + Ax_t + \varepsilon_t$  and backward dynamics  $x_t = A^\dagger x_{t+1} - A^\dagger a_0 - A^\dagger \varepsilon_t$  are  $\Sigma$  and  $A^\dagger \Sigma (A^\dagger)^T$ , respectively.  $\Sigma$  and  $A^\dagger \Sigma (A^\dagger)^T$  determine the approximate reversibility as  $\Gamma_\alpha$ . (b)  $\alpha = 1$  is often chosen to balance  $\Gamma_\alpha$ 's emphasis on both determinism and degeneracy. For  $\alpha < 1$ ,  $\Gamma_\alpha$  tends to capture more non-degeneracy of  $p(x_{t+1}|x_t)$ . For  $\alpha > 1$ ,  $\Gamma_\alpha$  emphasizes the determinism.

When  $A$  is irreversible or  $A^\dagger \Sigma (A^\dagger)^T, \Sigma > 0$ , the closer  $p(x_{t+1}|x_t)$  and  $p(x_t|x_{t+1})$  to Dirac distributions and  $A$  to a full-rank matrix, the stronger  $p(x_{t+1}|x_t)$ 's reversibility. Therefore, when the covariance of both forward and backward dynamics satisfy  $\Sigma \rightarrow 0$ ,  $A^\dagger \Sigma (A^\dagger)^T \rightarrow 0$  and  $A$  is close to a full-rank matrix,  $x_{t+1}, x_t$  are close to bijective and  $x_{t+1} = a_0 + Ax_t + \varepsilon_t \rightarrow Ax_t + a_0$ ,  $x_t = A^\dagger x_{t+1} - A^\dagger a_0 - A^\dagger \varepsilon_t \rightarrow A^\dagger x_{t+1} - A^\dagger a_0$  are approximate reversible dynamics. From this, we know that we need to find an indicator that includes both  $\Sigma$  and  $A^\dagger \Sigma (A^\dagger)^T$  to quantify the approximate reversibility of  $p(x_{t+1}|x_t)$  as shown in Fig.1. In the next subsection, we provide this indicator  $\Gamma_\alpha$ .

The results obtained in this section are also applicable to SDE and NN but require special processing. In Section 2.5.3, we will introduce application cases in NN, and in Section 4.1 and 4.2, we will specifically introduce the processing methods of nonlinear GIS and SDE to calculate SVD-based CE.

### 2.2.1 Definitions of $\Gamma_\alpha$

Similar to the framework in Zhang's article [25], to calculate approximate reversibility, it is necessary to obtain the singular value spectrum of TPM, and the same applies to GIS. For GIS, we need to treat  $p(x_{t+1}|x_t)$  as a TPM with continuous states and apply operations from functional analysis [47] to calculate its singular value spectrum. Firstly we calculate the Gaussian kernel which corresponds to  $P \cdot P^T$  of TPM in Subsection 2.1.2 when probability space is continuous as

$$\begin{aligned}
 K(\mathbf{x}, \mathbf{y}) &= \int_{-\infty}^{\infty} p(\mathbf{z}|\mathbf{x})p(\mathbf{z}|\mathbf{y})d\mathbf{z} \\
 &= (2\pi)^{-\frac{n}{2}} \det(2\Sigma)^{-\frac{1}{2}} \exp \left\{ -\frac{1}{4}(\mathbf{x} - \mathbf{y})^T (A^T \Sigma^{-1} A)(\mathbf{x} - \mathbf{y}) \right\} \\
 &\equiv \mathcal{K}(\mathbf{x} - \mathbf{y}).
 \end{aligned} \tag{2.16}$$

Suppose  $\zeta$  is a singular value of  $p(x_{t+1}|x_t)$ , then  $\zeta^2$  is the eigenvalue of  $K(\mathbf{x}, \mathbf{y}) = \mathcal{K}(\mathbf{x} - \mathbf{y})$  and  $\psi(\mathbf{x})$  is the eigenfunction corresponding to the eigenvalue  $\zeta^2$ . By analogy with the theorem of the spectrum of stochastic integral operators in functional analysis [47], we can derive  $\zeta^2$  by

$$(\mathbf{K}\psi)(\mathbf{x}) = \int_{-\infty}^{\infty} K(\mathbf{x}, \mathbf{y})\psi(\mathbf{y})d\mathbf{y} = \zeta^2\psi(\mathbf{x}). \tag{2.17}$$

Based on the properties of the Fourier transform of the convolution function in the integral transform, we can consider the above integral in Eq.(2.17) as a convolution of  $\mathcal{K}(\mathbf{y})$  and  $\psi(\mathbf{y})$ . Then the eigenvalue spectrum  $\zeta^2(\omega)$  in the frequency space is obtained through Fourier transform [48] as

$$\hat{\mathcal{K}}(\omega)\hat{\psi}(\omega) = \mathcal{F} \{ \mathcal{K}(\mathbf{y}) \} \mathcal{F} \{ \psi(\mathbf{y}) \} = \zeta^2\hat{\psi}(\omega). \tag{2.18}$$

From this, we can also obtain the singular value spectrum  $\zeta(\omega) = \sqrt{\hat{\mathcal{K}}(\omega)}$  of  $p(x_{t+1}|x_t)$  in the frequency space as  $\omega \in \mathcal{R}^n$ .

**Definition 2.3.** (*Approximate reversibility*): Suppose the singular value spectrum of GIS  $p(x_{t+1}|x_t) = \mathcal{N}(Ax_t + a_0, \Sigma)$  is  $\zeta(\omega)$ ,  $a_0, \omega, x_t, x_{t+1} \in \mathcal{R}^n$ ,  $A, \Sigma \in \mathcal{R}^{n \times n}$ , then the  $\alpha$ -ordered approximate dynamical reversibility of  $p(x_{t+1}|x_t)$  is defined as

$$\Gamma_\alpha \equiv \int_{-\infty}^{\infty} \zeta^\alpha(\omega) d\omega \quad (2.19)$$

where  $\alpha \in (0, 2]$ .

According to Definition 2.3, the approximate dynamical reversibility  $\Gamma_\alpha$  of GIS  $x_{t+1} = a_0 + Ax_t + \varepsilon_t, \varepsilon_t \sim \mathcal{N}(0, \Sigma)$  is given in Proposition 2.1. The detailed calculation process can be referred to Appendix A.2 in Supplementary Information.

**Proposition 2.1.** (*Approximate reversibility of GIS*): Suppose  $x_{t+1} = a_0 + Ax_t + \varepsilon_t, \varepsilon_t \sim \mathcal{N}(0, \Sigma)$  as the transitional probability from  $x_t \in \mathcal{R}^n$  to  $x_{t+1} \in \mathcal{R}^n$  in GIS as Equation (2.30), its  $\alpha$ -ordered singular value spectrum is:

$$\zeta^\alpha(\omega) = \{\det(\Sigma)^{\frac{1}{2}} \text{pdet}(A^T \Sigma^{-1} A)^{\frac{1}{2}}\}^{-\frac{\alpha}{2}} \exp\left\{-\frac{\alpha}{2} (\omega^T (A^T \Sigma^{-1} A)^\dagger \omega)\right\} \quad (2.20)$$

$\omega \in \mathcal{R}^n$ , the  $\alpha$ -ordered approximate dynamical reversibility of  $p(x_{t+1}|x_t)$  is defined as:

$$\Gamma_\alpha = \left(\frac{2\pi}{\alpha}\right)^{\frac{n}{2}} \text{pdet}(A^T \Sigma^{-1} A)^{\frac{1}{2} - \frac{\alpha}{4}} \det(\Sigma^{-1})^{\frac{\alpha}{4}}. \quad (2.21)$$

From Eq.(2.21) we know that  $\Gamma_\alpha$  is an indicator determined by the forward and backward covariance matrices  $\Sigma$  and  $A^\dagger \Sigma (A^\dagger)^T$  as shown in Fig.1a, which can be used as approximate reversibility in Definition 2.2. Similar to  $\mathcal{J}$ ,  $\Gamma_\alpha$  is also positively correlated with the absolute value of determinant  $|\det(A)|$  and negatively correlated with  $|\det(\Sigma)|$ . Therefore, it can be concluded that  $\Gamma_\alpha$  and  $\mathcal{J}$  are positively correlated in Theorem 2.1, which means  $\Gamma_\alpha$  can also be used to quantify the strength of causality as  $\mathcal{J}$ .  $\simeq$  in Eq.(2.22) and Eq.(2.33) represents 'approximately equal or equal to'. Detailed proof can be found in Appendix B in supplementary information.

**Theorem 2.1.** (*Correlation between  $\Gamma_\alpha$  and EI*): When the backward dynamics  $p(x_t|x_{t+1}) = \mathcal{N}(A^\dagger x_{t+1} - A^\dagger a_0, A^\dagger \Sigma (A^\dagger)^T)$  is closed to a normalized normal distribution as  $A^\dagger \Sigma (A^\dagger)^T \approx I_n$ ,  $\Gamma_\alpha$  and dimension averaged EI are positively correlated as

$$\ln \Gamma_\alpha \simeq n(1 - \frac{\alpha}{4}) \mathcal{J} + C. \quad (2.22)$$

$\ln \Gamma_\alpha$  is the reversible information and measures the degree of approximate reversibility.  $C = \frac{n}{2} \ln\left(\frac{2\pi}{\alpha}\right) - n(1 - \frac{\alpha}{4}) \ln\left(\frac{L}{\sqrt{2\pi e}}\right)$  is a constant term independent of  $A$  and  $\Sigma$ . When the backward dynamics  $p(x_t|x_{t+1})$  is a normalized normal distribution, i.e.  $A \in \mathcal{R}^{m \times n}$  is reversible and  $A^\dagger \Sigma (A^\dagger)^T = A^{-1} \Sigma (A^{-1})^T = I_n$ , the equal sign holds.

In the next subsection, we further demonstrate this conclusion by analyzing how determinism and degeneracy are reflected by  $\Gamma_\alpha$ . Since  $\Gamma_\alpha$  does not include the parameter  $L$ , which represents the size of the probability space with a uniform distribution that needs to be pre-set,  $\Gamma_\alpha$  is much stronger than the definition of  $\mathcal{J}$ .

## 2.2.2 Determinism and degeneracy

As pointed out by [25],  $\Gamma_\alpha$ 's reflection on determinism in Eq.(2.5) and degeneracy in Eq.(2.6) mainly depends on the transformation of hyperparameter  $\alpha$ . By adjusting the parameter  $\alpha \in (0, 2]$ , we can make  $\Gamma_\alpha$  reflect the **determinism** or **degeneracy** of  $p(x_{t+1}|x_t) = \mathcal{N}(Ax_t + a_0, \Sigma)$ .

As  $\alpha \rightarrow 0$ ,

$$\Gamma_{\alpha \rightarrow 0} \rightarrow \left(\frac{2\pi}{\alpha}\right)_{\alpha \rightarrow 0}^{\frac{n}{2}} \text{pdet}(A^T \Sigma^{-1} A)^{\frac{1}{2}}, \quad (2.23)$$

in which  $\text{pdet}(A^T \Sigma^{-1} A)$  is the Moore-Penrose generalized inverse matrix of  $A^\dagger \Sigma (A^\dagger)^T$ .  $A^\dagger \Sigma (A^\dagger)^T$  is the covariance matrix of the inverse dynamics  $x_t = A^\dagger x_{t+1} - A^\dagger a_0 - A^\dagger \varepsilon_t$  of  $x_{t+1} = a_0 + Ax_t + \varepsilon_t$ . In the calculation of  $\mathcal{J}$ , non-degeneracy  $\mathcal{J}_2$  in Eq.(2.6) describes how exactly we can infer the state  $x_{t-1}$  in previous time step from the current state  $x_t$  which is also the predictability of backward dynamics, so  $\Gamma_{\alpha \rightarrow 0}$  resembles the non-degeneracy term in the definition of  $\mathcal{J}$ . When  $\text{pdet}(A^T \Sigma^{-1} A)$  becomes smaller,  $p(x_{t+1}|x_t)$  becomes more degeneracy.

Similarly, as  $\alpha \rightarrow 2$ , since

$$\Gamma_2 = (\pi)^{\frac{n}{2}} \det(\Sigma^{-1})^{\frac{1}{2}}, \quad (2.24)$$

and covariance matrix  $\Sigma$  of  $x_{t+1} = a_0 + Ax_t + \varepsilon_t$  directly determine the determinism term  $\mathcal{J}_1$  in  $\mathcal{J}$  which measures how the current state  $x_t$  can deterministically influence the state  $x_{t+1}$  in next time step,  $\Gamma_2$  is comparable with the determinism term. An increase of  $\det(\Sigma^{-1})$  leads to higher maximum transition probabilities, reflecting stronger determinism in the underlying dynamics. When  $\det(\Sigma^{-1}) \rightarrow \infty$ ,  $p(x_{t+1}|x_t)$  approaches the Dirac distribution, the determinism will tend towards  $\infty$ .

In practice,  $\alpha = 1$  is often chosen to balance  $\Gamma_\alpha$ 's emphasis on both determinism and degeneracy. For  $\alpha < 1$ ,  $\Gamma_\alpha$  tends to capture more of the non-degeneracy of  $p(x_{t+1}|x_t)$ . In contrast, for  $\alpha > 1$ ,  $\Gamma_\alpha$  emphasizes the determinism of  $p(x_{t+1}|x_t)$ . Given the significance of  $\alpha = 1$ , we primarily present results for this case, and we will denote

$$\Gamma \equiv \Gamma_1 = (2\pi)^{\frac{n}{2}} \text{pdet}(A^T \Sigma^{-1} A)^{\frac{1}{4}} \det(\Sigma^{-1})^{\frac{1}{4}} \quad (2.25)$$

in the subsequent discussion.  $\Gamma_\alpha$  in three different scenarios are shown in Fig.1b.

### 2.2.3 Dimension averaged reversible information

Because  $\Gamma_\alpha$  is related to the dimensionality of the input variable and is influenced by a constant that is not related to the variable, we need to average the dimensionality of the input variable by taking the logarithm and subtract the constant term as dimension averaged reversible information to characterize dimensional independent approximate dynamical reversibility for a more reasonable comparison of iterative systems of different dimensions

**Definition 2.4.** (*Dimension averaged reversible information*): For  $\Gamma_\alpha$ , we can average the dimensionality of the input variable by taking the logarithm as

$$\gamma_\alpha \equiv \frac{1}{n} \ln \Gamma_\alpha \quad (2.26)$$

to get *the dimension averaged reversible information*.

Suppose  $r(\cdot)$  means the rank of matrix  $\cdot$  and  $s_i(\cdot)$  means the  $i$ -th singular value of matrix  $\cdot$ , and we denote  $r(A^T \Sigma^{-1} A) \equiv r$ ,  $r(\Sigma^{-1}) = n$ ,  $s_i(A^T \Sigma^{-1} A) \equiv s_i$  and  $s_i(\Sigma^{-1}) \equiv \kappa_i$ , we can get the expression form based on SVD as Proposition 2.2.

**Proposition 2.2.** *The dimension averaged reversible information subtracted from the constant term based on SVD is*

$$\hat{\gamma}_\alpha = \gamma_\alpha - \frac{1}{2} \ln \left( \frac{2\pi}{\alpha} \right) = \frac{1}{n} \left( \frac{1}{2} - \frac{\alpha}{4} \right) \sum_{i=1}^r \ln s_i + \frac{\alpha}{4n} \sum_{i=1}^n \ln \kappa_i. \quad (2.27)$$

$\hat{\gamma}_\alpha$  is only affected by the singular values of  $A^T \Sigma^{-1} A$  and  $\Sigma^{-1}$ .

Proposition 2.2 can directly manifests that  $\hat{\gamma}_\alpha$  and CE quantified by  $\Delta \Gamma_\alpha$  only depend on the SVD of  $A^T \Sigma^{-1} A$  and  $\Sigma^{-1}$ .  $\Delta \Gamma_\alpha$  is the index of SVD-based CE discussed in the next subsection.

## 2.3 SVD-based CE for GIS

One of the main contributions of this article is the new quantification of CE for GIS based on approximate dynamical reversibility under SVD following the definition of TPM in [25], which depends only on the system's parameters and does not require the optimization of coarse-graining strategies. Because  $\Gamma_\alpha$  is calculated based on generalized determinants  $\text{pdet}(A^T \Sigma^{-1} A)$ , removing zero singular values will not change the first term of  $\hat{\gamma}_\alpha$ . If  $r(A^T \Sigma^{-1} A) \equiv r < n$ , we can directly replace  $n$  with  $r$  to obtain the macro-state dimension averaged reversibility information as

$$\hat{\gamma}_\alpha(0) \equiv \frac{1}{r} \left( \frac{1}{2} - \frac{\alpha}{4} \right) \sum_{i=1}^r \ln s_i + \frac{\alpha}{4r} \sum_{i=1}^r \ln \kappa_i \quad (2.28)$$

and define clear causal emergence. Here, 0 in  $\hat{\gamma}_\alpha(0)$  is to conform in the same form as the definition of vague CE which will be clear in the following text. To ensure the Gaussianity of the system, we need to ensure that  $\Sigma$  is an invertible matrix, so clear CE only occurs when  $A$  is not full rank.

**Definition 2.5.** (Clear causal emergence): For a given GIS  $p(x_{t+1}|x_t) = \mathcal{N}(Ax_t + a_0, \Sigma)$ , if  $r = r(A^T \Sigma^{-1} A) < n$  then **clear causal emergence** occurs in this system. The degree of clear CE is

$$\Delta\Gamma_\alpha(0) \equiv \hat{\gamma}_\alpha(0) - \hat{\gamma}_\alpha = \frac{1}{r} \left( \frac{1}{2} - \frac{\alpha}{4} \right) \sum_{i=1}^r \ln s_i + \frac{\alpha}{4r} \sum_{i=1}^r \ln \kappa_i - \frac{1}{n} \left( \frac{1}{2} - \frac{\alpha}{4} \right) \sum_{i=1}^r \ln s_i - \frac{\alpha}{4n} \sum_{i=1}^n \ln \kappa_i. \quad (2.29)$$

However, clear CE is difficult to directly detect in reality because it is unlikely for the parameter matrix derived from the data to have strictly zero singular values. So it is difficult to find a strict non-full rank matrix, even if the singular value of  $A^T \Sigma^{-1} A$  is quite small and cannot be directly treated as a strict non-full rank matrix. On the other hand,  $\Sigma^{-1}$  may have very small singular values. So more often than not, we need to establish a lower bound for singular values as  $\epsilon$ , where only singular values  $s_i, \kappa_i \geq \epsilon$  are considered effective. Due to the information loss caused by deleted singular values  $s_i, \kappa_i \leq \epsilon$ ,  $\epsilon$  also determines the upper limit of the system's loss information. The number of effective singular values is called the effective rank  $r_\epsilon(A^T \Sigma^{-1} A)$  and  $r_\epsilon(\Sigma^{-1})$ . Based on global effective rank of the whole system as  $r_\epsilon = \min\{r_\epsilon(A^T \Sigma^{-1} A), r_\epsilon(\Sigma^{-1})\}$ , we can define vague macro reversibility as

$$\hat{\gamma}_\alpha(\epsilon) \equiv \frac{1}{r_\epsilon} \left( \frac{1}{2} - \frac{\alpha}{4} \right) \sum_{i=1}^{r_\epsilon} \ln s_i + \frac{\alpha}{4r_\epsilon} \sum_{i=1}^{r_\epsilon} \ln \kappa_i \quad (2.30)$$

and defined vague CE.

**Definition 2.6.** (Vague causal emergence): For a given random  $p(x_{t+1}|x_t) = \mathcal{N}(Ax_t + a_0, \Sigma)$ , suppose the singular values of  $A^T \Sigma^{-1} A$  are  $s_1 \geq s_2 \geq \dots \geq s_r \geq 0$ . For a given real value  $\epsilon \in [0, s_1]$  as a lower bound for singular values, if there is an integer  $i \in [1, r]$  such that  $s_i \equiv s_i(A^T \Sigma^{-1} A) > \epsilon$ , then there is **vague causal emergence** with the level of vagueness  $\epsilon$  occurred in the system. The same applies to handling  $\kappa_i, i = 1, \dots, n$ , of  $\Sigma^{-1}$ . We define **global effective rank**

$$r_\epsilon \equiv \min\{r_\epsilon(A^T \Sigma^{-1} A), r_\epsilon(\Sigma^{-1})\} \quad (2.31)$$

as  $r_\epsilon(A^T \Sigma^{-1} A) = \max\{i | s_i > \epsilon\}$  and  $r_\epsilon(\Sigma^{-1}) = \max\{i | \kappa_i > \epsilon\}$ . The degree of vague CE is:

$$\Delta\Gamma_\alpha(\epsilon) \equiv \hat{\gamma}_\alpha(\epsilon) - \hat{\gamma}_\alpha = \frac{1}{r_\epsilon} \left( \frac{1}{2} - \frac{\alpha}{4} \right) \sum_{i=1}^{r_\epsilon} \ln s_i + \frac{\alpha}{4r_\epsilon} \sum_{i=1}^{r_\epsilon} \ln \kappa_i - \frac{1}{n} \left( \frac{1}{2} - \frac{\alpha}{4} \right) \sum_{i=1}^r \ln s_i - \frac{\alpha}{4n} \sum_{i=1}^n \ln \kappa_i. \quad (2.32)$$

Under setting the level of vagueness  $\epsilon$  of singular values, vague CE can be calculated based on global effective rank  $r_\epsilon$ . It can be concluded that clear CE is a special form of vague CE as  $\epsilon = 0$ .

The following theorem can guarantee the rationality of quantifying CE using Definitions 2.5 and 2.6. According to Eq.(2.22),  $\Delta\Gamma_\alpha(\epsilon)$  and  $\Delta\mathcal{J}^*$  are approximately linear and positively correlated as shown in Theorem 2.2, which means that  $\Delta\Gamma_\alpha(\epsilon)$  can replace  $\Delta\mathcal{J}^*$  to get CE does not depend on coarse-graining.

**Theorem 2.2.** (Correlation between  $\Delta\Gamma_\alpha(\epsilon)$  and  $\Delta\mathcal{J}^*$ ): When the backward dynamics  $p(x_t|x_{t+1}) = \mathcal{N}(A^\dagger x_{t+1} - A^\dagger a_0, A^\dagger \Sigma (A^\dagger)^T)$  is closed to a normalized normal distribution as  $A^\dagger \Sigma (A^\dagger)^T \approx I_n$ ,  $\Delta\Gamma_\alpha(\epsilon)$  and  $\Delta\mathcal{J}^*$  are approximately linear and positively correlated as

$$\Delta\Gamma_\alpha(\epsilon) \simeq \left(1 - \frac{\alpha}{4}\right) \Delta\mathcal{J}^*. \quad (2.33)$$

The equal sign holds when the inverse dynamics  $p(x_t|x_{t+1}) = \mathcal{N}(A^\dagger x_{t+1} - A^\dagger a_0, A^\dagger \Sigma (A^\dagger)^T)$  is a normalized normal distribution as  $A^\dagger \Sigma (A^\dagger)^T = A^{-1} \Sigma (A^{-1})^T = I_n$ .

## 2.4 Coarse-graining strategy based on SVD

After learning that  $\Delta\Gamma_\alpha$  and  $\Delta\mathcal{J}^*$  are approximately positively correlated and only determined by the difference in singular values of  $A^T \Sigma^{-1} A$  and  $\Sigma^{-1}$ , we need to find the optimal coarse-graining strategy  $\phi(x_t) = Wx_t$  defined by  $W \in \mathcal{R}^{r_\epsilon \times n}$ , based on SVD, which is determined by the singular vectors of  $A^T \Sigma^{-1} A$  and  $\Sigma^{-1}$ . Since both  $A^T \Sigma^{-1} A$  and  $\Sigma^{-1}$  are symmetric matrices, the SVD of them are

$$\begin{aligned} A^T \Sigma^{-1} A &= USU^T \\ \Sigma^{-1} &= VKV^T. \end{aligned} \quad (2.34)$$



$S = \text{diag}(s_1, \dots, s_n)$  and  $K = \text{diag}(\kappa_1, \dots, \kappa_n)$ ,  $s_1 \geq \dots \geq s_n$ ,  $\kappa_1 \geq \dots \geq \kappa_n$ , are singular value matrices of  $A^T \Sigma^{-1} A$  and  $\Sigma^{-1}$ . Corresponding singular vector matrices  $U = (u_1, \dots, u_n)$  and  $V = (v_1, \dots, v_n)$ . Due to the filtering of singular values when calculating  $\Delta \Gamma_\alpha(\epsilon)$ , we need to redefine the singular vectors corresponding to the retained and discarded singular values during coarse-graining.

When  $r_\epsilon$  is fixed,  $s_1, \dots, s_{r_\epsilon}$  and  $\kappa_1, \dots, \kappa_{r_\epsilon}$  and their corresponding singular vectors need to be retained. We therefore decompose the orthogonal matrices  $U$  and  $V$  as

$$\begin{aligned} U &= (U_1, U_2), U_1 \in \mathcal{R}^{n \times r_\epsilon}, U_2 \in \mathcal{R}^{n \times (n-r_\epsilon)} \\ V &= (V_1, V_2), V_1 \in \mathcal{R}^{n \times r_\epsilon}, V_2 \in \mathcal{R}^{n \times (n-r_\epsilon)}, \end{aligned} \quad (2.35)$$

where  $U_1 = (u_1, \dots, u_{r_\epsilon})$ ,  $V_1 = (v_1, \dots, v_{r_\epsilon})$ , and  $U_2 = (u_{r_\epsilon+1}, \dots, u_n)$ ,  $V_2 = (v_{r_\epsilon+1}, \dots, v_n)$ , respectively. The effective rank  $r_\epsilon$  determines the dimensions of  $U_1$ ,  $U_2$ ,  $V_1$ , and  $V_2$ .

If  $W = U_1^T$ , from the perspective of the covariance matrix, coarse-graining  $\phi(x_t) = Wx_t$  can preserve the maximum singular value of  $A^T \Sigma^{-1} A$ . When  $W = V_1^T$ , we only need to change the analysis based on backward dynamics to forward dynamics.

However, the optimal coarse-graining strategy  $\phi(x_t) = Wx_t$  requires considering both  $A^T \Sigma^{-1} A$  and  $\Sigma^{-1}$  to balance forward and backward dynamics, so it is necessary to construct  $W$  based on the vectors of  $U = (u_1, \dots, u_n)$  and  $V = (v_1, \dots, v_n)$  together. Since  $U_1 \neq V_1$ , we generally cannot guarantee that  $s_i, \dots, s_{r_\epsilon}$  and  $\kappa_i, \dots, \kappa_{r_\epsilon}$  are retained together. Therefore, when constructing  $W$ , we need a classified discussion of the span spaces of  $U$  and  $V$ . Here we define the span space of matrix  $\cdot$  as  $\mathcal{M}(\cdot)$  and

$$\Omega_I = \mathcal{M}(U_1) \cap \mathcal{M}(V_1), \Omega_{II} = (\mathcal{M}(U_1) \cap \mathcal{M}(V_2)) \cup (\mathcal{M}(U_2) \cap \mathcal{M}(V_1)). \quad (2.36)$$

Since the dimension  $r_I$  of  $\Omega_I$  can be less than  $r_\epsilon$ , so if  $u_i \in \Omega_I$  and  $v_i \in \Omega_I$ , retaining the corresponding  $s_i$  or  $\kappa_i$  will not result in  $s_{j|u_j \in \mathcal{M}(U_2)}$  or  $\kappa_{j|v_j \in \mathcal{M}(V_2)}$  being retained together. However,  $u_i \in \Omega_{II}$  or  $v_i \in \Omega_{II}$  may cause  $s_{j|u_j \in \mathcal{M}(U_2)}$  or  $\kappa_{j|v_j \in \mathcal{M}(V_2)}$  being retained. Thus, we combine the vectors from  $\Omega_I$  and  $\Omega_{II}$  to construct the parameters  $W = (W_I^T, W_{II}^T)^T$  of the coarse-graining strategy, where  $W_I, W_{II}$  are constructed from  $\Omega_I$  and  $\Omega_{II}$ , respectively.

### (1) Collaborative coarse-graining

We first consider the coarse-graining strategy generated by  $\Omega_I$ . There is no conflict in the selection of  $s_i, \kappa_j > \epsilon$  when  $u_i, v_j \in \Omega_I$ , so we only need to calculate the orthogonal base vector of  $\Omega_I$ . All variables  $\beta$  in  $\Omega_I$  can be expressed simultaneously by  $U_1, V_1$ , that is we need to solve the following equation:

$$U_1 a = V_1 b, \quad (2.37)$$

and to force  $a, b \in \mathcal{R}^{r_\epsilon \times 1}$  and  $U_1 a = V_1 b \in \mathcal{R}^{n \times 1}$ ,  $a, b$  are coefficients of the linear combination of vectors in  $U_1, V_1$ . For this, we need to find the orthogonal base of the zero space of  $(U_1, -V_1)$  by

$$\begin{pmatrix} \mathcal{A} \\ \mathcal{B} \end{pmatrix} = \text{Schmidt}(\text{Null}(U_1, -V_1)) \in \mathcal{R}^{2r_\epsilon \times r_I}. \quad (2.38)$$

$\text{Null}(\cdot)$  represents the null space of matrix  $\cdot$ , while  $\text{Schmidt}(\cdot)$  represents the orthogonal base of the space  $\cdot$ . In this way, the parameters of the first part of the coarse-graining strategy, collaborative coarse-graining, can be directly calculated by

$$W_I^T = U_1 \mathcal{A} = V_1 \mathcal{B} \in \mathcal{R}^{n \times r_I} \quad (2.39)$$

and  $\Omega_I = \mathcal{M}(U_1 \mathcal{A}) = \mathcal{M}(V_1 \mathcal{B})$ . Due to  $\Omega_I \subset \mathcal{M}(U_1)$ ,  $r_I \leq r_\epsilon$ , to construct  $W \in \mathcal{R}^{r_\epsilon \times n}$ , we need to complete the rest part of  $W$  from the conflicting parts  $\Omega_{II}$ .

### (2) Prioritized coarse-graining

$\exists s_i, \kappa_j > \epsilon$ ,  $u_i, v_j \in \Omega_{II}$  indicates that the first  $r_I$  singular vectors, i.e. the vectors in  $\Omega_I$ , are not sufficient to span an  $r_\epsilon$  dimensional space, so  $r_{II} = r_\epsilon - r_I$  more orthogonal singular vectors are needed to be introduced to support this space. Therefore, it is necessary to add singular vectors  $u_i, v_j \in \Omega_{II}$  where  $\exists s_l, \kappa_m < \epsilon$ ,  $u_i, v_j \not\perp u_l, v_m$  which means the impact of  $s_l, \kappa_m$  will not be completely eliminated. This is the reason why the linear coarse-graining strategy cannot obtain the true  $\Delta \Gamma_\alpha(\epsilon)$  in all conditions. But we can prioritize selecting the maximum singular values  $s_i, \kappa_j > \epsilon$  corresponding to  $u_i, v_j \in \Omega_{II}$  to minimize the error. First, we arrange these singular values in descending order as

$$Q = (q_i | q_i \in \mathbf{S}), \quad (2.40)$$

where  $\mathbf{S} = \{s_i, \kappa_j | u_i, v_j \in \Omega_2\}$  and  $q_1 \geq q_2 \geq \dots$ . Secondly, we select the first  $r_{\text{II}}$  singular values as  $\hat{Q} = (q_1, \dots, q_{r_{\text{II}}})$  and perform Schmidt orthogonalization on their corresponding singular vectors to obtain additional parameters

$$W_{\text{II}}^T = \text{Schmidt}(u_i|_{s_i \in \hat{Q}}, v_i|_{\kappa_i \in \hat{Q}}) \in \mathcal{R}^{n \times r_{\text{II}}}. \quad (2.41)$$

By concatenating the parameter matrices obtained from the two coarse-graining strategies,  $W$  of the final coarse-graining strategy  $\phi(x_t) = Wx_t$  can be obtained by

$$W = \begin{pmatrix} W_{\text{I}} \\ W_{\text{II}} \end{pmatrix} \in \mathcal{R}^{r_\epsilon \times n}. \quad (2.42)$$

When  $\Sigma = \sigma^2 I$  or  $\Omega_{\text{II}} = \emptyset$ , our parameter is equivalent to  $W = U_{\text{I}}^T$ .

## 2.5 Experiments

In this subsection, we will provide three numerical experimental examples to show the conceptions and conclusions derived in previous sections. The first two are for GIS with known models, and the third one is the application applied on a neural network trained by the time series data generated by a Susceptible-Infected-Recovere (SIR) model.

### 2.5.1 Malthusian growth models

The first example contains 4 variables, in which the first two variables  $x_1, x_2$  follow the Malthusian growth model [49] with different growth rates of 0.2 and 0.05. To study CE, we define the other two variables  $x_3, x_4$  as the copies of the first two variables shown as Fig.2a, thus, they are redundant dimensions. If  $x = (x_1, x_2, x_3, x_4)$ , the evolution of  $x$  is a GIS  $x_{t+1} = a_0 + Ax_t + \varepsilon_t, \varepsilon_t \sim \mathcal{N}(0, \sigma^2 I_4)$  as  $x_t, x_{t+1} \in \mathcal{R}^4, \sigma^2 = 0.1, a_0 = 0$ , and

$$A = \begin{pmatrix} 1.2 & 0 & 0 & 0 \\ 0 & 1.05 & 0 & 0 \\ 1.2 & 0 & 0 & 0 \\ 0 & 1.05 & 0 & 0 \end{pmatrix}. \quad (2.43)$$

A sample of evolutionary trajectories generated by this model is shown in Fig.2b. In this model,  $\Sigma = \sigma^2 \cdot I_4$  is a full rank matrix, so we only need to study the backward dynamics covariance matrix  $A^T \Sigma^{-1} A$  (Fig.2c). This matrix only has two singular values as the singular value spectrum is shown in Fig.2e with  $r = 2 < 4$ , the horizontal axis represents the sequence number of singular values arranged in descending order as  $s_1 \geq \dots \geq s_4$ , while the vertical axis represents the magnitude of singular values  $s_i$ , so clear CE can be calculated as  $\Delta \Gamma_\alpha(0) = 0.4034$ . Fig.2g shows the coarse-graining parameter  $W \in \mathcal{R}^{2 \times 4}$  obtained by truncating the orthogonal matrix  $U$  after SVD of  $A^T \Sigma^{-1} A$ . When clear CE exists, variables  $x_1$  and  $x_2$  hold all the relevant information contained within  $x_3$  and  $x_4$ . Therefore, the role of  $\phi(x) = Wx$  is to remove the last two dimensions and only retain the first two dimensions of  $x$  to describe the evolution of the growth model.

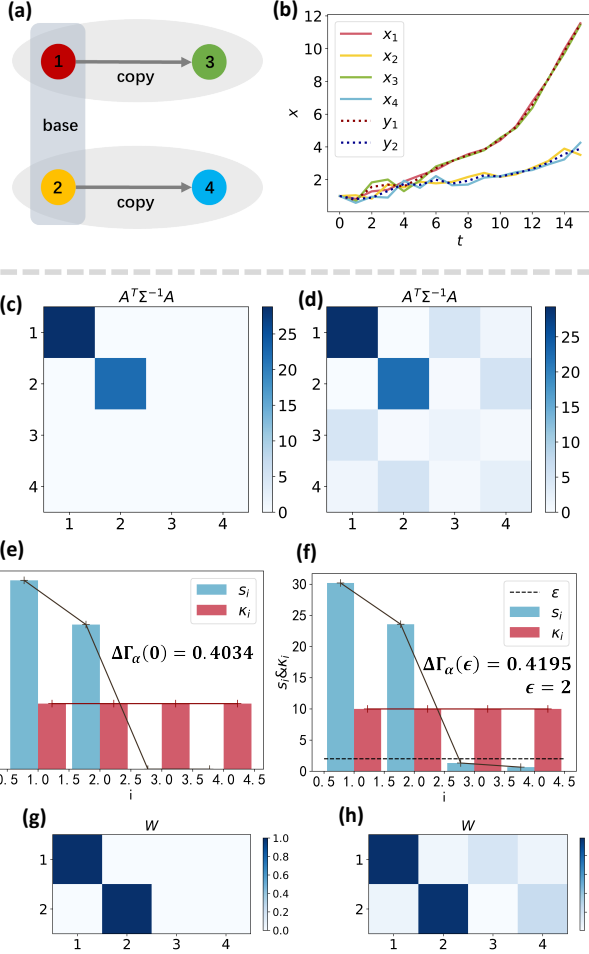
To show the concept of vague CE, we can add some perturbations to  $A$  and obtain

$$A = \begin{pmatrix} 1.2 & 0 & 0 & 0 \\ 0 & 1.05 & 0.001 & 0 \\ 1.22 & 0 & 0.4 & 0.1 \\ 0 & 1.06 & 0.03 & 0.5 \end{pmatrix} \quad (2.44)$$

and  $A^T \Sigma^{-1} A$  (Fig.2d) is a full rank matrix as  $r = n = 4$ . Then clear CE  $\Delta \Gamma_\alpha(0) = 0$ . However, by observing the singular value spectrum in Fig.2f, we can see that only two dimensions have significant impacts, so we need to calculate vague CE. By using the threshold selection as  $\epsilon = 2$ , vague CE can be calculated as  $\Delta \Gamma_\alpha(\epsilon) = 0.4195$ . The coarse-graining parameter  $W$  is shown in Fig.2h, the columns represent the macroscopic dimensions, and the rows represent the microscopic dimensions. Due to disturbances,  $x_3$  and  $x_4$  also contain some independent information.  $\phi(x) = Wx, W = U_{\text{I}}^T$ , is to merge  $x_1$  and  $x_3, x_2$  and  $x_4$  by weighted summation and the two row-vectors that make up  $W$  are exactly equal to the singular vectors corresponding to the two largest singular values  $s_1, s_2$ .

This case illustrates that sometimes high dimensions may reduce the efficiency of reversibility of a system due to dimensional redundancy. Retaining only the maximum  $r_\epsilon$  singular values of the covariance matrix can improve the efficiency of reversibility and generate CE.

## Malthusian growth models



## Discretized Brownian motion

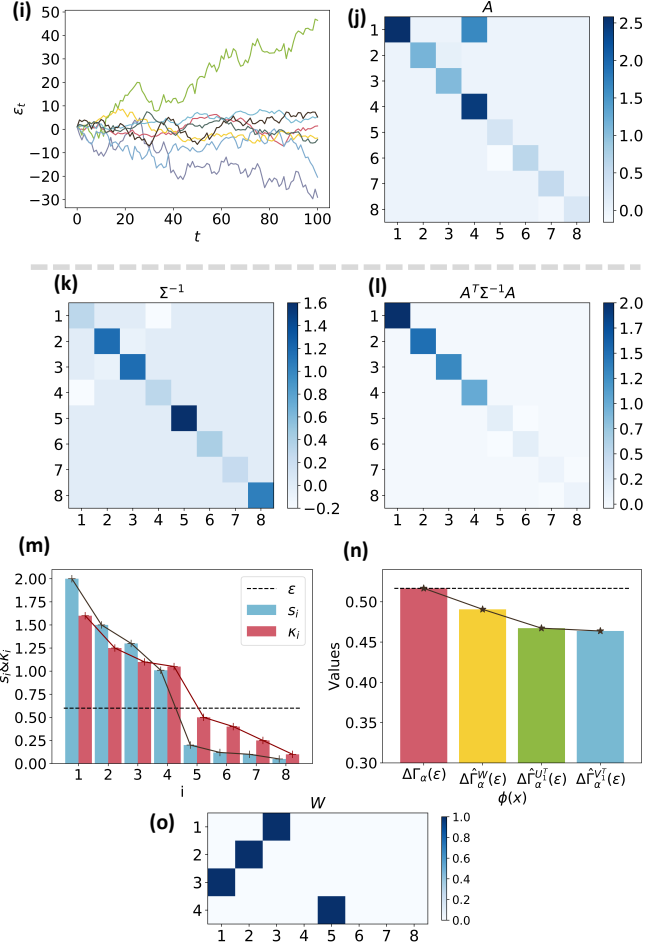


Figure 2: Analytical solutions obtained from numerical simulations of known models. (a) A Malthusian growth mode where  $x_3, x_4$  are copies of  $x_1, x_2$ . (b) A sample of trajectory generated by the Malthusian growth models with growth rates of 0.2 and 0.05.  $x_i, i = 1, 2, 3, 4$ , are micro-states, while  $y_1$  and  $y_2$  are theoretical macro-states obtained by coarse-graining. (c) The backward dynamics covariance matrix  $A^T \Sigma^{-1} A$  when  $r(A) = 2$ . (d)  $A^T \Sigma^{-1} A$  after random perturbations to  $A$ . (e) The singular value spectrum of  $A^T \Sigma^{-1} A$  and  $\Sigma^{-1}$  when  $A^T \Sigma^{-1} A$  only has two singular values. Clear CE can be calculated as  $\Delta \Gamma_\alpha(0) = 0.4034$ . (f) The singular value spectrum of  $A^T \Sigma^{-1} A$  and  $\Sigma^{-1}$  when  $A$  is perturbed. The degree of Vague CE is  $\Delta \Gamma_\alpha(\epsilon) = 0.4195$  when  $\epsilon = 2$ . (g) Coarse-graining parameter  $W$  obtained by truncating  $U$  in the presence of Clear CE, the number of columns represents the macroscopic dimension, and the number of rows represents the microscopic dimension. (h) The coarse-graining parameter  $W$  for vague CE case, the first macro-state dimension is determined by  $x_1, x_3$ , and the first macro-state dimension is determined by  $x_2, x_4$ . (i) The samples of trajectories of the noise term  $\varepsilon_t$  in Brownian motion. (j) Parameter  $A$  of the drift vector  $\mu = a_0 + Ax_t$ . (k) and (l) show the inverse of the covariance matrix of forward and backward dynamics, which is  $\Sigma^{-1}$  and  $A^T \Sigma^{-1} A$ . (m) Singular value spectrums of  $\Sigma^{-1}$  and  $A^T \Sigma^{-1} A$  with  $\epsilon = 0.6$ . (n) Approximate CE based on SVD  $\Delta \Gamma_\alpha^W(\epsilon) = \hat{\gamma}_\alpha^W(\epsilon) - \gamma_\alpha = 0.4907$ , which is close to the true value  $\Delta \Gamma_\alpha(\epsilon) = 0.5167$ .  $\Delta \Gamma_\alpha^W(\epsilon)$  obtained by  $\phi(x_t) = Wx_t$  is closer to the true value  $\Delta \Gamma_\alpha(\epsilon)$  than  $\Delta \Gamma_\alpha^{U^T}(\epsilon)$  or  $\Delta \Gamma_\alpha^{V_1^T}(\epsilon)$  which directly use  $\phi(x_t) = U_1^T x_t$  or  $\phi(x_t) = V_1^T x_t$ . (o) The optimal coarse-graining strategy parameter matrix  $W$ , which preserves the non-conflicting 3rd and 4th dimensions, along with the 1st and 5th dimensions with larger singular values  $\kappa_1$  and  $s_1$

## 2.5.2 Discretized Brownian motion

The design of this example is to demonstrate the need to simultaneously filter for singular values of  $\Sigma^{-1}$  and  $A^T \Sigma^{-1} A$ . Discretized Brownian motion is an approximation of continuous Brownian motion in discrete time, which is always used for numerical simulation and stochastic process modeling. Eq.(2.2) can be regarded as a discrete version method of the Ornstein Uhlenbeck (OU) [50] process. In this model,  $\mu = a_0 + Ax_t$  is the drift vector, which influences the evolution of the state,  $A$  is given as

$$A = \begin{pmatrix} 2.5819 & 0 & 0 & 1.6411 & 0 & 0 & 0 & 0 \\ 0 & 1.1298 & 0.0672 & 0 & 0 & 0 & 0 & 0 \\ 0 & 0 & 1.0539 & 0 & 0 & 0 & 0 & 0 \\ 0 & 0 & 0 & 2.4617 & 0 & 0 & 0 & 0 \\ 0 & 0 & 0 & 0 & 0.3162 & 0 & 0 & 0 \\ 0 & 0 & 0 & 0 & -0.1581 & 0.6123 & 0 & 0 \\ 0 & 0 & 0 & 0 & 0 & 0 & 0.5477 & 0 \\ 0 & 0 & 0 & 0 & 0 & 0 & -0.0890 & 0.2519 \end{pmatrix}, \quad (2.45)$$

and  $a_0 = 0$ . Covariance matrix  $\Sigma$  representing the diffusion coefficient, which determines the magnitude and correlation of random fluctuations across dimensions of  $\varepsilon_t$  like Fig.2i.

As we set  $A$  as shown in Fig.2j, after perform SVD on  $\Sigma^{-1}$  and  $A^T \Sigma^{-1} A$  in Fig.2k and Fig.2l according to Eq.(2.34), we can obtain singular vector matrices  $U = (u_1, \dots, u_n)$  and  $V = (v_1, \dots, v_n)$  as

$$U = \begin{pmatrix} 1 & 0 & 0 & 0 & 0 & 0 & 0 & 0 \\ 0 & 1 & 0 & 0 & 0 & 0 & 0 & 0 \\ 0 & 0 & 1 & 0 & 0 & 0 & 0 & 0 \\ 0 & 0 & 0 & 1 & 0 & 0 & 0 & 0 \\ 0 & 0 & 0 & 0 & \frac{1}{\sqrt{2}} & \frac{1}{\sqrt{2}} & 0 & 0 \\ 0 & 0 & 0 & 0 & -\frac{1}{\sqrt{2}} & \frac{1}{\sqrt{2}} & 0 & 0 \\ 0 & 0 & 0 & 0 & 0 & 0 & \frac{1}{\sqrt{2}} & \frac{1}{\sqrt{2}} \\ 0 & 0 & 0 & 0 & 0 & 0 & -\frac{1}{\sqrt{2}} & \frac{1}{\sqrt{2}} \end{pmatrix}, V = \begin{pmatrix} 0 & 0 & 0 & 0 & \frac{1}{\sqrt{2}} & 0 & 0 & \frac{1}{\sqrt{2}} \\ 0 & \frac{1}{\sqrt{2}} & \frac{1}{\sqrt{2}} & 0 & 0 & 0 & 0 & 0 \\ 0 & -\frac{1}{\sqrt{2}} & \frac{1}{\sqrt{2}} & 0 & 0 & 0 & 0 & 0 \\ 0 & 0 & 0 & 0 & -\frac{1}{\sqrt{2}} & 0 & 0 & \frac{1}{\sqrt{2}} \\ 1 & 0 & 0 & 0 & 0 & 0 & 0 & 0 \\ 0 & 0 & 0 & 0 & 0 & 1 & 0 & 0 \\ 0 & 0 & 0 & 0 & 0 & 0 & 1 & 0 \\ 0 & 0 & 0 & 1 & 0 & 0 & 0 & 0 \end{pmatrix} \quad (2.46)$$

and diagonal matrix of singular values

$$S = \text{diag}(2, 1.5, 1.3, 1.01, 0.2, 0.12, 0.1, 0.05) \quad (2.47)$$

$$K = \text{diag}(1.6, 1.25, 1.1, 1.05, 0.5, 0.4, 0.25, 0.1).$$

After obtaining the singular value spectrum in Fig.2m, we specify  $\epsilon = 0.6$  to get  $\Delta\Gamma_\alpha(\epsilon) = 0.5167$  and the number of macro-states is  $r_\epsilon = 4$ . To obtain theoretical values  $\Delta\Gamma_\alpha(\epsilon) = 0.5167$ ,  $s_1, \dots, s_4$  and  $\kappa_1, \dots, \kappa_4$  should be retained.

As we get the singular value spectrum of  $\Sigma^{-1}$  and  $A^T \Sigma^{-1} A$  Fig.2m, we can also calculate the coarse-graining strategy based on SVD. First, we calculate the parameter  $W_I$  of collaborative coarse-graining. According to Eq.(2.38), we get the orthogonal product of the zero space of  $(U_1, -V_1)$  as

$$\mathcal{A} = \begin{pmatrix} 0 & 0 \\ 0 & 1 \\ 1 & 0 \\ 0 & 0 \end{pmatrix}, \mathcal{B} = \begin{pmatrix} 0 & 0 \\ -\frac{1}{\sqrt{2}} & \frac{1}{\sqrt{2}} \\ \frac{1}{\sqrt{2}} & \frac{1}{\sqrt{2}} \\ 0 & 0 \end{pmatrix}. \quad (2.48)$$

Then we can get

$$W_I^T = U_1 \mathcal{A} = V_1 \mathcal{B} \in \mathcal{R}^{n \times r_1} \quad (2.49)$$

which is also the orthogonal base of  $\Omega_I$  as  $r_I = 2$ . By observing the matrix in Eq.(2.46), we can find that it satisfies  $u_2, u_3, v_2, v_3 \in \Omega_I$  as  $\Omega_I = \mathcal{M}(U_1 \mathcal{A}) = \mathcal{M}(V_1 \mathcal{B}) = \mathcal{M}(u_2, u_3) = \mathcal{M}(v_2, v_3)$  exactly holds.

At the same time, by comparing the values of  $u_i V_2$  and  $v_i U_2$ ,  $u_i \in \mathcal{M}(U_1)$ ,  $v_i \in \mathcal{M}(V_1)$ , we can know

$$u_1, u_4, v_1, v_4 \in \Omega_{II} \quad (2.50)$$

as  $\Omega_{II} = \mathcal{M}(u_1, u_4, v_1, v_4)$  and

$$Q = (s_1, \kappa_1, \kappa_4, s_4). \quad (2.51)$$

Since  $r_{\text{II}} = r_{\epsilon} - r_{\text{I}} = 2$  and  $\hat{Q} = (s_1, \kappa_1)$ . the parameters of the prioritized coarse-graining are

$$W_{\text{II}}^T = (u_1, v_1). \quad (2.52)$$

Because  $u_1^T v_1 = 0$ , we do not need to repeat Schmidt orthogonalization. According to Eq.(2.42), we can obtain the optimal coarse-graining strategy parameter matrix  $W$  in Fig.2o, which preserves the non-conflicting 3rd and 4th dimensions, along with the 1st and 5th dimensions with larger singular values  $\kappa_1$  and  $s_1$ . So in reality, we retained  $s_1, s_2, s_3, s_5$  and  $\kappa_1, \kappa_2, \kappa_3, \kappa_5$ .

The macro-state dynamics obtained through  $\phi = Wx_t$  has approximate reversibility  $\hat{\gamma}_{\alpha}^W(\epsilon)$ . Through it, we can obtain an approximate CE based on SVD  $\Delta\Gamma_{\alpha}^W(\epsilon) = \hat{\gamma}_{\alpha}^W(\epsilon) - \gamma_{\alpha} = 0.4907$ , which is close to true  $\Delta\Gamma_{\alpha}(\epsilon) = 0.5167$ . By comparing in Fig.2n, we can see that  $\Delta\Gamma_{\alpha}^W(\epsilon)$  obtained by  $\phi(x_t) = Wx_t$  is closer to the true value  $\Delta\Gamma_{\alpha}(\epsilon)$  than  $\Delta\Gamma_{\alpha}^{U_1^T}(\epsilon)$  or  $\Delta\Gamma_{\alpha}^{V_1^T}(\epsilon)$  which directly use  $\phi(x_t) = U_1^T x_t$  or  $\phi(x_t) = V_1^T x_t$  and only consider one direction in forward and backward dynamics.

### 2.5.3 SIR based on NN

Most systems in reality are unable to obtain precise dynamic models to calculate analytical solutions for CE as demonstrated in the previous two examples. However, we can train a neural network to obtain approximate dynamics by observed time series data. Our third case is to show the phenomenon of CE obtained by a well-trained neural network (NN) on the training time series data generated by a Susceptible-Infected-Recovered (SIR) dynamical model [51] as shown in Fig.3b with the following dynamics:

$$\begin{cases} \frac{dS}{dt} = -\beta SI, \\ \frac{dI}{dt} = \beta SI - \gamma I, \\ \frac{dR}{dt} = \gamma I, \end{cases} \quad (2.53)$$

as shown in Fig.3a, where  $S, I, R \in [0, 1]$  represent the rate of susceptible, infected, and recovered individuals in a population,  $\beta = 1$  and  $\gamma = 0.5$  are parameters for infection and recovery rates.

To generate the time series data of the micro-state, we adopt the same method in our previous work of NIS+[19]. We generate data by converting  $dS/dt, dI/dt$  into  $\Delta S/\Delta t, \Delta I/\Delta t$  as  $\Delta t = 0.01$  and  $(S_{t+\Delta t}, I_{t+\Delta t}) \approx (S_t, I_t) + (dS_t/dt, dI_t/dt)\Delta t$ . Then we duplicate the macro-state  $(S_t, I_t)$  as shown in Fig.3c and added Gaussian random noise to form the micro-state  $x_t$  as

$$x_t = (S_t, I_t, S_t, I_t) + \xi_t, \quad (2.54)$$

where  $\xi_t \sim N(0, \Sigma)$  and

$$\Sigma = \sigma \begin{pmatrix} 1 & -\frac{1}{2} & 0 & 0 \\ -\frac{1}{2} & 1 & 0 & 0 \\ 0 & 0 & 1 & -\frac{1}{2} \\ 0 & 0 & -\frac{1}{2} & 1 \end{pmatrix}. \quad (2.55)$$

as  $\sigma = 0.04$ .

By feeding the micro-state data into a forward neural network (NN) called **Covariance Learner Network**, we can use this model to approximate the micro-dynamics of the SIR model. The model we trained has the following structure:

- **Input layer:** The NN has  $n = 4$  input neurons, corresponding to the size of the input vector  $x_t$ .
- **Hidden layers:** The network contains two hidden layers. The first hidden layer has *hidden\_size* = 64 neurons, followed by a *LeakyReLU* activation function. The second hidden layer also has *hidden\_size* = 64 neurons, followed by another *LeakyReLU* activation.
- **Output layer:** The output layer contains two parts. The first part,  $f_{\mu}$ , outputs a mean vector  $\mu$  of size  $n$ . The second part,  $f_L$ , outputs the elements of the lower triangular part of the Cholesky decomposition of the covariance matrix, with size  $n \times n$ .

Formally, given an input, the network applies a series of transformations:

$$\begin{aligned} h_1 &= \text{LeakyRELU}(B_1 x_t + b_1), \\ h_2 &= \text{LeakyRELU}(B_2 h_1 + b_2), \\ \mu &= B_{\mu} h_2 + b_{\mu}, \\ L_{\Sigma} &= B_L h_2 + b_L, \end{aligned} \quad (2.56)$$

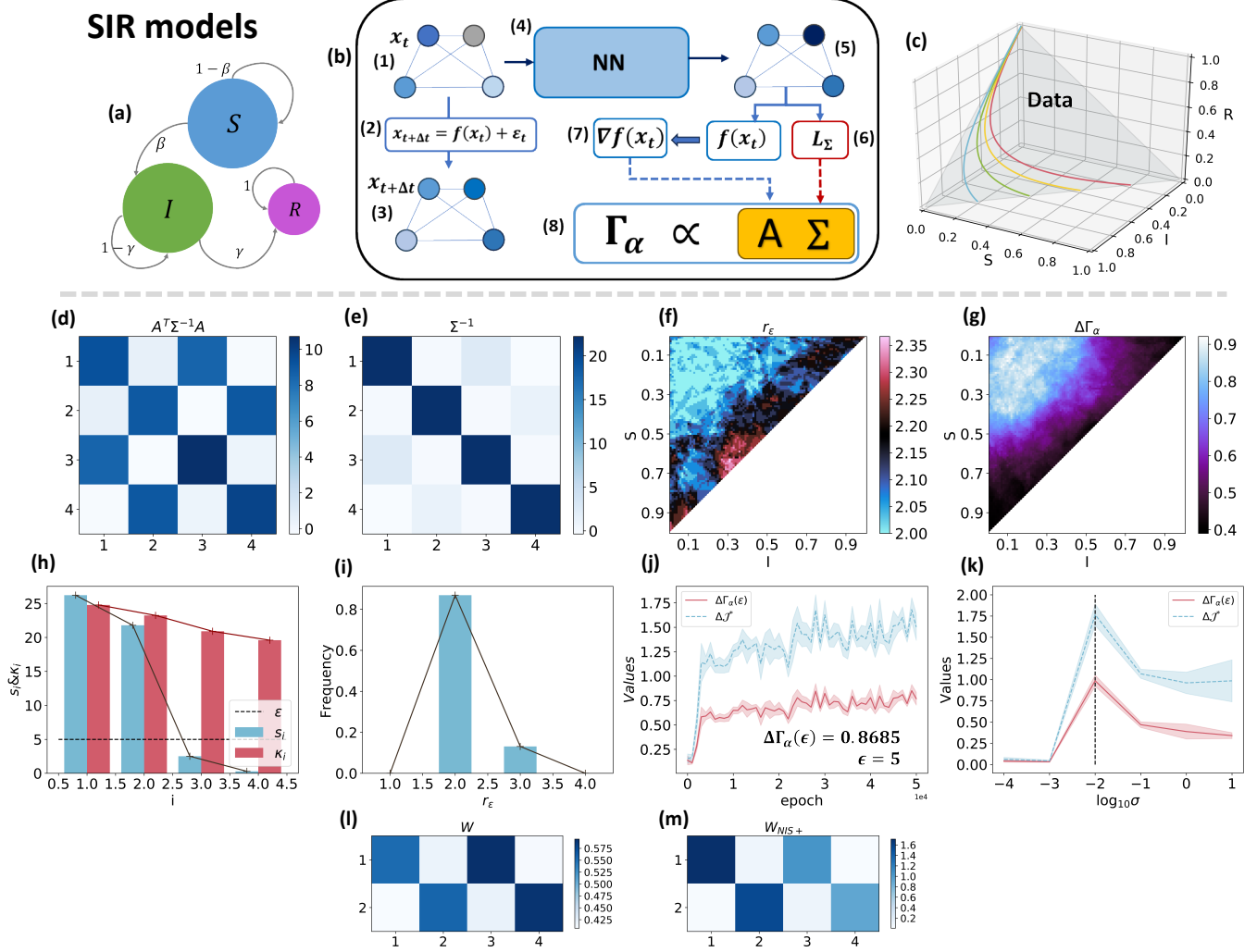


Figure 3: Numerical solution obtained by training SIR model with simple NN. (a) SIR model. (b) The processing process of NN. (1) and (3) are the variables  $x_t$  and  $x_{t+\Delta t}$  at adjacent time points. (2) Dynamical model. (4) Simple NN model. (5) After inputting  $x_t$ , NN predicts  $x_{t+\Delta t}$  as  $\hat{x}_{t+\Delta t}$ . (6)  $A(x_t)$  is the Jacobian matrix of the trained model at  $x_t$ . (7)  $\Sigma(x_t)$  is the co-variance matrix estimated by the mean square error of  $x_{t+\Delta t}$ . (8) The numerical solution of  $\Gamma_\alpha$ . (c) Training data as NIS+. (d) The numerical solution of  $A^T \Sigma^{-1} A$  in NN trained SIR model. (e) The numerical solution of  $\Sigma^{-1}$  in NN trained SIR model. (f) Distribution of  $r_\epsilon$  in sample space (SIR) with different ( $S, I$ ). (g) Distribution of  $\Delta \Gamma_\alpha$  under different ( $S, I$ ). (h) The singular value spectrum of  $A^T \Sigma^{-1} A$  and  $\Sigma^{-1}$  in NN trained SIR model. (i) The frequency of  $r_\epsilon$  under different samples  $A^T(x_t) \Sigma^{-1}(x_t) A(x_t)$ . (j) Maximum  $\Delta \Gamma_\alpha(\epsilon) = 0.8685$  when the training period is around 50,000 as  $\epsilon = 5$ . (k) The changing trend of CE under different  $\sigma$ , the threshold for trend change is around  $\sigma = 0.01$ . (l) The coarse-graining matrix  $W$  for NN. (m) The coarse-graining matrix  $W_{NIS+}$  of NIS+.

where  $B$  and  $b$  denote trainable weight matrices and biases. The predicted  $f(x_t)$  and final covariance matrix is then computed as:

$$\begin{aligned} f(x_t) &= \mu, \\ \Sigma &= L_{\Sigma} L_{\Sigma}^T. \end{aligned} \tag{2.57}$$

Since the quantification of our CE framework does not require a pre-setting coarse-grained strategy and the coarse-grained function can be directly obtained from the singular value decomposition of  $A^T \Sigma^{-1} A$  after setting  $r_{\epsilon}$ , we can directly calculate the degree of CE by  $\Delta \Gamma_{\alpha}$  and ignore the learning processes of encoder, decoder and macro-dynamics in NIS+ as mentioned in [19]. Due to the nonlinearity of the SIR dynamics, we cannot directly use the CE quantification method of linear GIS. Instead, we approximate NN as a linear mapping at different input  $x_t$  by Taylor expansion (see the method Section 4). We can obtain the CE identification result and the final coarse-graining strategy directly by calculating  $A(x_t) = \nabla f(x_t)$  as the Jacobian matrix of the trained NN model at  $x_t$ . And  $\Sigma(x_t)$  is the covariance matrix that neural networks can directly output. Due to the differences under different  $x_t$ , we can randomly generate  $x_t$  with a uniform distribution on the domain of the SIR dynamics and take the average value as  $A^T \Sigma^{-1} A \approx \langle A^T(x_t) \Sigma^{-1}(x_t) A(x_t) \rangle_{x_t}$  and  $\Sigma^{-1} \approx \langle \Sigma^{-1}(x_t) \rangle_{x_t}$  to calculate  $\Delta \Gamma_{\alpha}$  of the system. Fig.3b visualizes the method of computation for  $\Delta \Gamma$  on a multivariate Gaussian model.

Using the data in Fig.3c, we can perform SVD on matrices  $A^T \Sigma^{-1} A$  and  $\Sigma^{-1}$  in Fig.3d and Fig.3e. In Figure Fig.3h, we can see the singular value spectrum of matrices  $A^T \Sigma^{-1} A$  and  $\Sigma^{-1}$  in which the horizontal axis represents the sequence number of singular values arranged in descending order, while the vertical axis represents the magnitude of singular values  $s_i, \kappa_i$ . Due to the existence of the copy operation, even the simplest NN can recognize only two dimensions with larger singular values as  $r_{\epsilon} = 2$  when  $\epsilon = 5$ . If we directly calculate  $r_{\epsilon}$  by  $A^T(x_t) \Sigma^{-1}(x_t) A(x_t)$  as  $x_t$  is sampled from the test data set and plot  $r_{\epsilon}$  as a matrix related to  $S, I$  in Fig.3f, we can see that most positions satisfy  $r_{\epsilon} = 2$ . By calculating the frequency of  $r_{\epsilon}$  under different samples  $A^T(x_t) \Sigma^{-1}(x_t) A(x_t)$ , from Fig.3i we can find that  $r_{\epsilon} = 2$  has the highest frequency.

From Fig.3h,  $A^T \Sigma^{-1} A$  has two larger singular values and  $r_{\epsilon} = 2$  as  $\epsilon = 5$ . In model training, we get the value of Vague CE as  $\Delta \Gamma_{\alpha}(\epsilon) = 0.8685$  when the training period is 50,000 which is shown in Fig.3j. We can also directly calculate  $\Delta \Gamma_{\alpha}(\epsilon)$  by  $A^T(x_t) \Sigma^{-1}(x_t) A(x_t)$  as  $x$  is sampled from the test data set and plot  $\Delta \Gamma_{\alpha}$  as a matrix related to  $S, I$  in Fig.3g. Comparing Fig.3f and Fig.3g, we can see that the most stable region of  $r_{\epsilon}$  and the region with the highest  $\Delta \Gamma_{\alpha}(\epsilon)$  are almost identical as  $(S, I)$  roughly located within a circle with a radius of 0.5 and a center of  $(0, 0)$ .

We can also compare the results of our framework and NIS+ mentioned in [19]. From figure Fig.3l and Fig.3m, we can see that the coarse-graining matrix  $W$  obtained through the singular vectors and the Jacobian matrix  $W_{NIS+}$  of the NIS+ coarse-graining encoder are similar. Both coarse-graining methods indicate that the first and the third micro-state dimensions mainly influence the first macro-state dimension, while the second and fourth micro-state dimensions mainly influence the second macro-state dimension. Both the values of  $W$  and  $W_{NIS+}$  are consistent with the copy method (Fig.2a) which is used during data generation. In addition, we can test the changing trend of CE under different  $\sigma$ . From Fig.3k, When  $\sigma < 0.01$ ,  $\Delta \Gamma_{\alpha}(\epsilon)$  is positively correlated with  $\sigma$ , and when  $\sigma > 0.01$ , the two are negatively correlated. We can see that the turning point for CE is around  $\sigma = 0.01$ , which is consistent with the value of obtained by NIS+ [19].

However, our framework addresses the decline in training efficiency associated with encoder training in NIS+, leading to a more streamlined and effective approach to model training and CE detection.

### 3 Discussion and conclusion

This article presents the approximate reversibility  $\Gamma_{\alpha}$  as a new exact quantification of CE for GIS.  $\Gamma_{\alpha}$  only depends on the singular values of forward and backward dynamic covariances  $\Sigma$  and  $A^{\dagger} \Sigma (A^{\dagger})^T$  without requiring predefined coarse-graining strategies  $\phi(x) = Wx$ . By retaining only the maximum  $r_{\epsilon}$  singular values of  $\Sigma^{-1}$  and  $A^T \Sigma^{-1} A$ , we can directly quantify CE of the system as  $\Delta \Gamma_{\alpha}$ . Better than EI-based CE, approximate reversibility with SVD directly provides accurate CE, which significantly improves accuracy and computational efficiency in both analytical solution computation and NN machine learning.

At the same time, we can directly obtain the optimal  $W$  based on the singular vectors matrix of two covariance matrices. This method balancing the conflict between preserving singular values in  $\Sigma^{-1}$  and  $A^T \Sigma^{-1} A$  while also calculating  $\Delta \Gamma_{\alpha}(\epsilon)$  closer to theoretical values. From the directly obtained  $W$ , we can see more clearly the strategies for aggregating micro-states into macro-states, where highly correlated dimensions can be aggregated and dimensions with too small singular values can be discarded.

Compared to the SVD-based CE of TPM,  $\Delta\Gamma_\alpha$  for GIS offers clearer insights into the correlation between SVD-based and EI-based CE. Both indicators correlate positively with  $A$  and negatively with  $\Sigma$ . We also reveal how parameter  $\alpha$  affects determinacy and degeneracy. Although these results can be obtained through numerical simulations on TPM, it is difficult to directly prove the underlying reasons without the help of GIS. Moreover, since most real-world data exist in continuous spaces rather than binary distributions, studying SVD-based CE in GIS has broader applicability.

In addition to the concept of reversible quantification of CE itself, another important innovation is the object of SVD. Previously, SVD in complex systems research mainly focused on data or dynamic parameters, often disregarding random noise as mere error. Our work focuses on covariance matrices, and the covariance matrix of inverse dynamics  $A^\dagger\Sigma(A^\dagger)^T$  precisely contains both the dynamic parameters  $A$  and the covariance of forward dynamics  $\Sigma$ . Whether calculating CE or deriving coarse-graining strategies, we consider both the dynamics and randomness of the system.

While our approach has made progress, several challenges remain unresolved. The first limitation is that our model is currently restricted to linear GIS, with nonlinear GIS approximated in a locally linear form. However, this approximation introduces stability issues, as the gradient of nonlinear functions may be ill-conditioned. In particular, cases where  $\nabla f(x) = 0$  or  $\nabla f(x) \rightarrow \infty$  lead to the breakdown of our framework. To address this, incorporating higher-order derivatives as a refined CE metric warrants further investigation.

The second issue arises when time is continuous rather than discrete, the existing CE quantification lacks objective formulations. The approach in this study discretizes time, converting differential equations into difference equations, where the choice of hyperparameter  $\Delta t$  strongly influences CE. As  $\Delta t \rightarrow 0$ , state transitions  $x_t \rightarrow x_{t+\Delta t}$  exhibit minimal variation, causing the rate of change to vanish. For continuous-time stochastic differential equations, a more principled CE measure is required to account for infinitesimal evolution dynamics.

The third issue is that both SVD-based and EI-based CE quantification methods require training an NN to infer dynamics when the governing equations are unknown. However, NN-based approaches are data-dependent and prone to parameter estimation errors, particularly in capturing interdimensional correlations. In our case, a multivariate Gaussian model approximates both the dynamical function and covariance. Yet, under high noise or limited data, the learned dynamics may deviate from the true system, leading to unreliable CE estimates. For systems with unknown models, it is crucial to develop representations that jointly approximate both the underlying dynamics and noise structure.

Future work will focus on optimizing the existing framework and extending its application to more complex systems. In numerical simulations, machine learning can be leveraged to learn intricate dynamical models, such as Vicsek and Kuramoto, which are analytically intractable. This allows for data-driven CE estimation and the exploration of its relationship with critical states. Additionally, our approach can be applied to real-world datasets, such as meteorological and EEG data, to identify practical problems where CE provides meaningful insights.

## 4 Methods

### 4.1 Nonlinear dynamics

Most of the analysis in the article is based on linear models, but there are also many nonlinear iterative models in reality. We can apply our framework to nonlinear models under certain conditions. Nonlinear stochastic iterative systems like  $x_{t+1} = f(x_t) + \varepsilon_t$ ,  $\varepsilon_t \sim \mathcal{N}(0, \Sigma)$ ,  $x_t \in \mathcal{R}^n$ ,  $\Sigma \in \mathcal{R}^{n \times n}$ , do not have the same known parameter matrix  $A$  as linear stochastic iterative systems. However, when  $f : \mathcal{R}^n \rightarrow \mathcal{R}^n$  and spatially continuous, the Taylor expansion  $f(x) = f(x') + \nabla f(x')(x - x') + o(x - x')$  is very similar to linear function  $Ax$  around  $x'$ . By using the definition that  $A$  is the slope, we can obtain an approximate expression of  $A_{x'}$  when  $x \approx x'$  as

$$A(x') = \frac{f(x) - f(x')}{x - x'} \approx \nabla f(x'). \quad (4.1)$$

So when iterative models are nonlinear, we can replace  $A$  with the gradient matrix as  $A(x_t) = \nabla f(x_t) \in \mathcal{R}^{n \times n}$  at  $x_t$  to calculate  $\Delta\mathcal{J}$  or  $\Delta\Gamma_\alpha$ . Since causal emergence is related to  $x_t$ , to determine the CE of the entire system, we can take the average of  $A$  and  $A^T\Sigma^{-1}A$  in  $x_t$ 's space  $\mathcal{X}$  as

$$A = \frac{1}{|\mathcal{X}|} \int_{\mathcal{X}} \nabla f(x_t) dx_t \quad (4.2)$$

and

$$A^T\Sigma^{-1}A = \frac{1}{|\mathcal{X}|} \int_{\mathcal{X}} \nabla f(x_t)^T \Sigma^{-1}(x_t) \nabla f(x_t) dx_t \quad (4.3)$$

to calculate the CE of the entire system,  $|\mathcal{X}|$  represents the size of  $\mathcal{X}$  and  $\Sigma(x_t)$  is the covariance at  $x_t$ .



## 4.2 Stochastic differential equations

Another case requiring special handling is time-continuous systems, where Fokker-plank equations describe dynamics [52] as

$$\frac{\partial p(x_t)}{\partial t} = -\nabla \cdot \left[ f(x_t)p(x_t) - \frac{1}{2}\Sigma\nabla p(x_t) \right], \quad (4.4)$$

or equivalent stochastic differential equations [27] as

$$\frac{dx_t}{dt} = f(x_t) + \Sigma^{\frac{1}{2}}\varepsilon_t \quad (4.5)$$

which is also expressed as  $dx_t = f(x_t)dt + \Sigma^{\frac{1}{2}}dW_t$ , where  $x_t \in \mathcal{R}^n$ ,  $\varepsilon_t = dW_t/dt \in \mathcal{R}^n$  and  $dW_t \sim \mathcal{N}(0, dtI_n)$ . We can approximate the differential of Brownian motion  $W_t \in \mathcal{R}^n$  as  $dW_t \approx \sqrt{dt}1_n$ ,  $1_n = (1, \dots, 1)_n^T$ .

The common method for dealing with this situation is to use finite difference  $\Delta x_t$  approximation for differentiation [53]  $dx_t$  as  $\Delta x_t = f(x_t)\Delta t + \Sigma^{\frac{1}{2}}\Delta W_t \sim \mathcal{N}(f(x_t)\Delta t, \Delta t\Sigma)$ . In this way, we can also approximate the stochastic differential equation in the form of a GIS as

$$x_{t+\Delta t} \approx x_t + \Delta x_t \sim \mathcal{N}(x_t + f(x_t)\Delta t, \Delta t\Sigma). \quad (4.6)$$

We can calculate CE by setting  $A = I_n + \nabla f(x_t)\Delta t$  and covariance  $\Delta t\Sigma \in \mathcal{R}^{n \times n}$ . Due to the need for discretization in continuous models in machine learning, this method can also provide a reference for the effectiveness of machine learning models. However this method has a big problem in that the  $\Delta t$  has a significant impact on the calculation of CE.

Ao et al. [26, 28] presented that through a transformation to a force equation, decomposition of the SDE into three components: potential function  $f(x_t)$ , dissipative matrix  $R(x_t)$ , and transverse matrix  $T(x_t)$  as

$$[R(x_t) + T(x_t)]\frac{dx_t}{dt} = -\nabla f(x_t) + R^{\frac{1}{2}}(x_t)\varepsilon_t. \quad (4.7)$$

$\nabla f(x_t)$  and  $R(x_t)$  happen to be highly correlated in their impact on our matrix  $A$  and  $\Sigma$ . So in the future, we can try to find more effective methods just based on three components to find a CE quantization scheme that does not rely on  $\Delta t$ .

## 4.3 System and observation noises

The noise  $\varepsilon \sim \mathcal{N}(0, \Sigma)$  in our model  $y = Ax + \varepsilon$  can be decomposed into system noise  $e$  and observation noise  $\xi$ . For the GIS like  $\mathbf{y} = A\mathbf{x} + e$ ,  $e \sim \mathcal{N}(0, E)$  is pure noise inherent in the system,  $\mathbf{y} \in \mathcal{R}^n$  follows a normal distribution about  $\mathbf{x} \in \mathcal{R}^n$ , so  $\mathbf{y} \sim \mathcal{N}(A\mathbf{x}, E)$ ,  $A \in \mathcal{R}^{n \times n}$ ,  $E \in \mathcal{R}^{n \times n}$ . We can add observation noise as

$$x = \mathbf{x} + \xi_{\mathbf{x}}, \xi_{\mathbf{x}} \sim \mathcal{N}(0, \Xi_{\mathbf{x}}) \quad (4.8)$$

$$y = \mathbf{y} + \xi_{\mathbf{y}}, \xi_{\mathbf{y}} \sim \mathcal{N}(0, \Xi_{\mathbf{y}}) \quad (4.9)$$

Since  $\mathbf{y} = A\mathbf{x} + e$ ,  $y = A(x - \xi_{\mathbf{x}}) + e + \xi_{\mathbf{y}} \sim \mathcal{N}(Ax_t, \Xi_{\mathbf{y}} + A\Xi_{\mathbf{x}}A' + E) = \mathcal{N}(Ax_t + a_0, \Sigma)$ , in which

$$\Sigma = \Xi_{\mathbf{y}} + A\Xi_{\mathbf{x}}A' + E \in \mathcal{R}^{n \times n} \quad (4.10)$$

is the combination of covariance matrixes of system and observation noises and

$$\varepsilon = -A\xi_{\mathbf{x}} + e + \xi_{\mathbf{y}} \in \mathcal{R}^n \quad (4.11)$$

is the combination of two types of noise. In real data,  $\Xi$  is more common than  $E$  and it's difficult to distinguish between the two directly. The SIR model in Eq.(2.54) used in this article only has observation noise  $\xi$  and the first two cases only have system noises  $e$ , all included in  $\varepsilon$ .

**Data Availability Statement:** All the codes and data are available at: [https://github.com/kilovoltage/SVD-based\\_CE\\_Gaussian](https://github.com/kilovoltage/SVD-based_CE_Gaussian).

## References

- [1] S. E. Jørgensen and F. Müller, “Ecosystems as complex systems,” *Handbook of Ecosystem Theories and Management. CRC Press LLC, Boca Raton*, pp. 5–20, 2000.
- [2] R. T. Wicks, S. C. Chapman, and R. Dendy, “Mutual information as a tool for identifying phase transitions in dynamical complex systems with limited data,” *Physical Review E*, vol. 75, no. 5, p. 051125, 2007.
- [3] C. Hartman and B. Benes, “Autonomous boids,” *Computer Animation and Virtual Worlds*, vol. 17, no. 3-4, pp. 199–206, 2006.
- [4] S. Jingnan, J. He, and X. Gao, “Neurofeedback training of control network improves ssvep-based bci performance in children,” 2021.
- [5] O. Sporns, J. Faskowitz, A. S. Teixeira, S. A. Cutts, and R. F. Betzel, “Dynamic expression of brain functional systems disclosed by fine-scale analysis of edge time series,” *Network Neuroscience*, vol. 5, no. 2, pp. 405–433, 2021.
- [6] T. F. Varley, *Uncovering Higher-Order Structures in Complex Systems with Multivariate Information Theory*. Indiana University, 2023.
- [7] Z. Zhao, Y. Zhou, B. Liu, J. He, J. Zhao, Y. Cai, J. Fan, X. Li, Z. Wang, Z. Lu, *et al.*, “Two-photon synthetic aperture microscopy for minimally invasive fast 3d imaging of native subcellular behaviors in deep tissue,” *Cell*, vol. 186, no. 11, pp. 2475–2491, 2023.
- [8] T. Dong, J. He, S. Wang, L. Wang, Y. Cheng, and Y. Zhong, “Inability to activate rac1-dependent forgetting contributes to behavioral inflexibility in mutants of multiple autism-risk genes,” *Proceedings of the National Academy of Sciences*, vol. 113, no. 27, pp. 7644–7649, 2016.
- [9] L. Ma, X.-D. Yang, F. Yang, X.-J. Zhou, and Z.-W. Wu, “Unveiling the early stage evolution of local atomic structures in the crystallization process of a metallic glass,” *Chinese Physics B*, vol. 33, no. 3, p. 036402, 2024.
- [10] H. S. Bennett and J. J. Filliben, “A systematic approach for multidimensional, closed-form analytic modeling: minority electron mobilities in ga1-xalxas heterostructures,” *Journal of Research of the National Institute of Standards and Technology*, vol. 105, no. 3, p. 441, 2000.
- [11] G. Tononi and O. Sporns, “Measuring information integration,” *BMC neuroscience*, vol. 4, pp. 1–20, 2003.
- [12] E. P. Hoel, L. Albantakis, and G. Tononi, “Quantifying causal emergence shows that macro can beat micro,” *Proceedings of the National Academy of Sciences*, vol. 110, no. 49, pp. 19790–19795, 2013.
- [13] E. P. Hoel, “When the map is better than the territory,” *Entropy*, vol. 19, no. 5, p. 188, 2017.
- [14] F. E. Rosas, P. A. M. Mediano, H. J. Jensen, A. K. Seth, A. B. Barrett, R. L. Carhart-Harris, and D. Bor, “Reconciling emergences: An information-theoretic approach to identify causal emergence in multivariate data,” *PLoS Computational Biology*, vol. 16, p. e1008289, Dec 2020.
- [15] L. Barnett and A. K. Seth, “Dynamical independence: discovering emergent macroscopic processes in complex dynamical systems,” *Physical Review E*, vol. 108, no. 1, p. 014304, 2023.
- [16] B. Yuan, J. Zhang, A. Lyu, J. Wu, Z. Wang, M. Yang, K. Liu, M. Mou, and P. Cui, “Emergence and causality in complex systems: A survey of causal emergence and related quantitative studies,” *Entropy*, vol. 26, no. 2, p. 108, 2024.
- [17] E. P. Hoel, L. Albantakis, W. Marshall, and G. Tononi, “Can the macro beat the micro? integrated information across spatiotemporal scales,” *Neuroscience of Consciousness*, vol. 2016, no. 1, p. niw012, 2016.
- [18] J. Zhang and K. Liu, “Neural information squeezer for causal emergence,” *Entropy*, vol. 25, no. 1, p. 26, 2022.
- [19] M. Yang, Z. Wang, K. Liu, Y. Rong, B. Yuan, and J. Zhang, “Finding emergence in data by maximizing effective information,” *National Science Review*, p. nwae279, 2024.
- [20] K. Liu, B. Yuan, and J. Zhang, “An exact theory of causal emergence for linear stochastic iteration systems,” *Entropy*, vol. 26, no. 8, 2024.

- [21] P. L. Williams and R. D. Beer, “Nonnegative decomposition of multivariate information,” *arXiv preprint arXiv:1004.2515*, 2010.
- [22] A. I. Luppi, P. A. Mediano, F. E. Rosas, D. J. Harrison, R. L. Carhart-Harris, D. Bor, and E. A. Stamatakis, “What it is like to be a bit: an integrated information decomposition account of emergent mental phenomena,” *Neuroscience of consciousness*, vol. 2021, no. 2, p. niab027, 2021.
- [23] J. Song and S. Ermon, “Understanding the limitations of variational mutual information estimators,” 2020.
- [24] C. Kaplanis, P. Mediano, and F. Rosas, “Learning causally emergent representations,” in *NeurIPS 2023 workshop: Information-Theoretic Principles in Cognitive Systems*, 2023.
- [25] J. Zhang, R. Tao, K. H. Leong, M. Yang, and B. Yuan, “Dynamical reversibility and a new theory of causal emergence based on SVD,” *npj Complexity*, vol. 2, p. 3, Jan. 2025.
- [26] P. Ao, “Emerging of stochastic dynamical equalities and steady state thermodynamics from darwinian dynamics,” *Communications in theoretical physics*, vol. 49, no. 5, p. 1073, 2008.
- [27] L. C. Evans, *An introduction to stochastic differential equations*, vol. 82. American Mathematical Soc., 2012.
- [28] R. Yuan, Y. Tang, and P. Ao, “Sde decomposition and a-type stochastic interpretation in nonequilibrium processes,” *Frontiers of Physics*, vol. 12, pp. 1–9, 2017.
- [29] Y. Sun, G. Hu, Y. Zhang, B. Lu, Z. Lu, J. Fan, X. Li, Q. Deng, and X. Chen, “Eigen microstates and their evolutions in complex systems,” *Communications in Theoretical Physics*, vol. 73, no. 6, p. 065603, 2021.
- [30] G. Hu, T. Liu, M. Liu, W. Chen, and X. Chen, “Condensation of eigen microstate in statistical ensemble and phase transition,” *Science China Physics, Mechanics & Astronomy*, vol. 62, pp. 1–8, 2019.
- [31] K. Gallivan, E. Grimme, and P. Van Dooren, “Asymptotic waveform evaluation via a lanczos method,” *Applied Mathematics Letters*, vol. 7, no. 5, pp. 75–80, 1994.
- [32] S. Gugercin, “An iterative svd-krylov based method for model reduction of large-scale dynamical systems,” *Linear Algebra and its Applications*, vol. 428, no. 8-9, pp. 1964–1986, 2008.
- [33] A. C. Antoulas, “An overview of approximation methods for large-scale dynamical systems,” *Annual reviews in Control*, vol. 29, no. 2, pp. 181–190, 2005.
- [34] J. Xue, J. Li, and Y. Gong, “Restructuring of deep neural network acoustic models with singular value decomposition,” in *Interspeech*, pp. 2365–2369, 2013.
- [35] J. Zhang, Q. Lei, and I. Dhillon, “Stabilizing gradients for deep neural networks via efficient svd parameterization,” in *International Conference on Machine Learning*, pp. 5806–5814, PMLR, 2018.
- [36] M. M. Bejani and M. Ghatee, “Theory of adaptive svd regularization for deep neural networks,” *Neural Networks*, vol. 128, pp. 33–46, 2020.
- [37] W. Dunsmuir and E. J. Hannan, “Vector linear time series models,” *Advances in Applied Probability*, vol. 8, no. 2, pp. 339–364, 1976.
- [38] B. Klein and E. Hoel, “The emergence of informative higher scales in complex networks,” *Complexity*, vol. 2020, pp. 1–12, 2020.
- [39] P. Chvykov and E. Hoel, “Causal geometry,” *Entropy*, vol. 23, no. 1, p. 24, 2020.
- [40] R. Comolatti and E. Hoel, “Causal emergence is widespread across measures of causation,” *arXiv preprint arXiv:2202.01854*, 2022.
- [41] E. Hoel, *The world behind the world: Consciousness, Free Will, and the Limits of Science*. Simon and Schuster, 2024.
- [42] J. C. A. Barata and M. S. Hussein, “The moore–penrose pseudoinverse: A tutorial review of the theory,” *Brazilian Journal of Physics*, vol. 42, pp. 146–165, 2012.
- [43] R. A. Horn and C. R. Johnson, *Matrix analysis*. Cambridge university press, 2012.

- [44] E. J. Hannan and L. Kavalieris, “Multivariate linear time series models,” *Advances in Applied Probability*, vol. 16, no. 3, pp. 492–561, 1984.
- [45] M. A. Lifshits, *Gaussian random functions*, vol. 322. Springer Science & Business Media, 2013.
- [46] M. Baldiotti, R. Fresneda, and J. Gazeau, “Dirac distribution and dirac constraint quantizations,” *Physica Scripta*, vol. 90, no. 7, p. 074039, 2015.
- [47] P. D. Lax, *Functional analysis*. John Wiley & Sons, 2014.
- [48] R. N. Bracewell, “The fourier transform,” *Scientific American*, vol. 260, no. 6, pp. 86–95, 1989.
- [49] O. Galor and D. N. Weil, “Population, technology, and growth: From malthusian stagnation to the demographic transition and beyond,” *American economic review*, vol. 90, no. 4, pp. 806–828, 2000.
- [50] R. A. Maller, G. Müller, and A. Szimayer, “Ornstein–uhlenbeck processes and extensions,” *Handbook of financial time series*, pp. 421–437, 2009.
- [51] J. Satsuma, R. Willox, A. Ramani, B. Grammaticos, and A. S. Carstea, “Extending the sir epidemic model,” *Physica A: Statistical Mechanics and its Applications*, vol. 336, no. 3-4, pp. 369–375, 2004.
- [52] D. Maoutsa, S. Reich, and M. Opper, “Interacting particle solutions of fokker–planck equations through gradient–log–density estimation,” *Entropy*, vol. 22, no. 8, p. 802, 2020.
- [53] N. Ikeda, S. Watanabe, M. Fukushima, and H. Kunita, *Itô’s stochastic calculus and probability theory*. Springer Science & Business Media, 2012.